GEOPHYSICS, VOL. 50, NO. 4 (APRIL 1985); P. 551 570, 31 FIGS., 2 TABLES.

Elastic-wave velocities and attenuation in an underground granitic repository for nuclear waste

B. N. P. Paulsson*, N. G. W. Cook‡, and T. V. McEvilly§

ABSTRACT

The behavior of a quartz monzonite rock mass subjected to a thermal load from emplaced canisters with electric heaters simulating high-level nuclear waste was monitored by a cross-hole seismic technique in a drift 340 m below the surface in the Stripa mine facility in Sweden. Traveltimes and amplitudes of 20 to 60 kHz ultrasonic compressional (P) and shear (S) waves were measured over the experiment duration of 750 days, on 2 to 4 m paths between four diamond-drilled boreholes around a heater. The signals were transmitted between the boreholes in six different directions and at different depths. Path-averaged P- and S-wave velocities were obtained from the times of flight of pulses of acoustic waves between separate P- and S-wave piezoelectric transmitter and receiver crystals. The attenuation Q^{-1} was obtained by a spectral ratio technique. When the heater was turned on, the P- and S-wave velocities increased to 4 and 10 percent, respectively, and stabilized at the elevated values. The P-wave velocities along a particular profile were found to increase linearly with the mean temperatures in the profiles sampled. These mean temperatures increased 25° to 55°C during the course of the experiment. When the heater was turned off after 398 days of heating, the velocities decreased with temperature and finally reached levels in most cases below those observed prior to heating the rock. The highest thermal stress close to the heater was estimated at 55 MPa. Q_α values increased throughout the heating interval, reaching changes of up to 60 percent shortly after turning off the heater. The Q values reveal no direct correlation with temperature or the closely associated thermal stress, although these phenomena clearly are driving the variation in Q. There is strong evidence relating attenuation properties to fracture closure and pore pressure changes associated with draining of the rock mass.

INTRODUCTION

Since 1977 the Stripa mine in central Sweden has been operated as an underground experimental site by the Swedish Nuclear Fuel Safety Program (Karnbranslesakerhet) under auspices of the parent organization, the Swedish Nuclear Fuel Supply Company (Svensk Karnbransleforsorjning), and the U.S. Department of Energy, through the University of California, Lawrence Berkeley Laboratory. The program had several experimental tasks, which have been described by Witherspoon and Degerman (1978), Witherspoon et al. (1980), and others.

The main objective at Stripa was to conduct three different heater experiments, and to collect information on the behavior of a granitic rock mass heated by electric heaters emplaced in boreholes of large diameter in the floor of an underground drift. The full-scale electric heaters were intended to simulate radioactive waste canisters with heat outputs of 3.6 kW (heater H9) and 5.0 kW (heater H10). Part of the radioactive waste research program was concerned with development and evaluation of geophysical techniques for the investigation of rock masses. One of these cross-hole, high-frequency, elastic-wave measurements—was used over a period of two-and-a-half years to monitor the rock mass around a 5.5 m deep, 406 mm diameter borehole (H9) in which a 3 m long 3.6 kW heater had been emplaced. The experiment was performed 340 m below the surface in a mined drift as shown in Figure 1. The drift is 6 m wide and 5 m high. A special smooth-wall blasting technique was used to minimize the influence of the blast effects on the experiment (Andersson and Halen, 1979).

A structural floor plan of the drift around heater H9 is shown in Figure 2. Also shown are the positions of four 10 m long by 56 mm diameter vertical seismic boreholes drilled in the vicinity

Manuscript received by the Editor November 31, 1983; revised manuscript received August 13, 1984.
*Formerly Engineering Geoscience, University of California, Berkeley; presently Chevron Oil Field Research Co., P. O. Box 446, LaHabra, CA 90631.
‡Department of Materials Science and Engineering, Earth Sciences Division, Lawrence Berkeley Laboratory, University of California, Berkeley, CA 94720.
§Department of Geology and Geophysics, Earth Sciences Division, Lawrence Berkeley Laboratory, University of California, Berkeley, CA 94720.

of the heater. The geology in the experimental drift was described in detail by Paulsson et al. (1981). Chan et al. (1980) described the thermal and thermomechanical data collected in the instrumentation holes.

The first objective of the ultrasonic cross-hole experiment was to investigate the feasibility of a high-frequency seismic technique to monitor the effects of changes in stress or temperature on the physical properties of the rock between pairs of boreholes. The second objective was to investigate the sensitivity of the technique for three-dimensional mapping of the physical properties of this rock. The seismic technique is appealing in that it is nondestructive and in that measurements of the rock properties can be performed in boreholes at a distance from the site. The advantage of the cross-hole technique over conventional downhole techniques is that the seismic signal travels largely under in-situ rock conditions while the downhole signal travels near the disturbed zone of the borehole wall.

The Stripa experiments, along with the associated extensive logging and mapping, provide an unparalleled opportunity to perform a well-controlled test of seismic field methods. Similar experiments were described in Fehler (1982) and Aki et al. (1982). However, the Stripa experiment was on a smaller scale and was more intensely instrumented and more carefully mapped than those of either Fehler or Aki et al. The scale of this detailed investigation in the field closed the gap between the laboratory tests and full-scale field work. In many respects this small-scale, well-controlled field experiment is the logical extension of laboratory tests.

EXPERIMENT SETTING— GEOLOGY AND FRACTURE DISTRIBUTION

The age of the Stripa quartz monzonite was reported as 1.69×10^9 years by Wollenberg et al. (1981). The quartz monzonite is associated with a series of pegmatite and aplite dikes. The youngest of the dikes are the steeply dipping diabase dikes with a north-northeast strike. The test area is dominated by a reddish, medium-grained, massive quartz monzonite, with an average grain size of 3 mm and a composition determined by point counting as indicated in Table 1 (Wollenberg et al., 1981).

The Stripa quartz monzonite is classified as serorogenic, differing from the preorgenic or synorogenic granitic rocks in

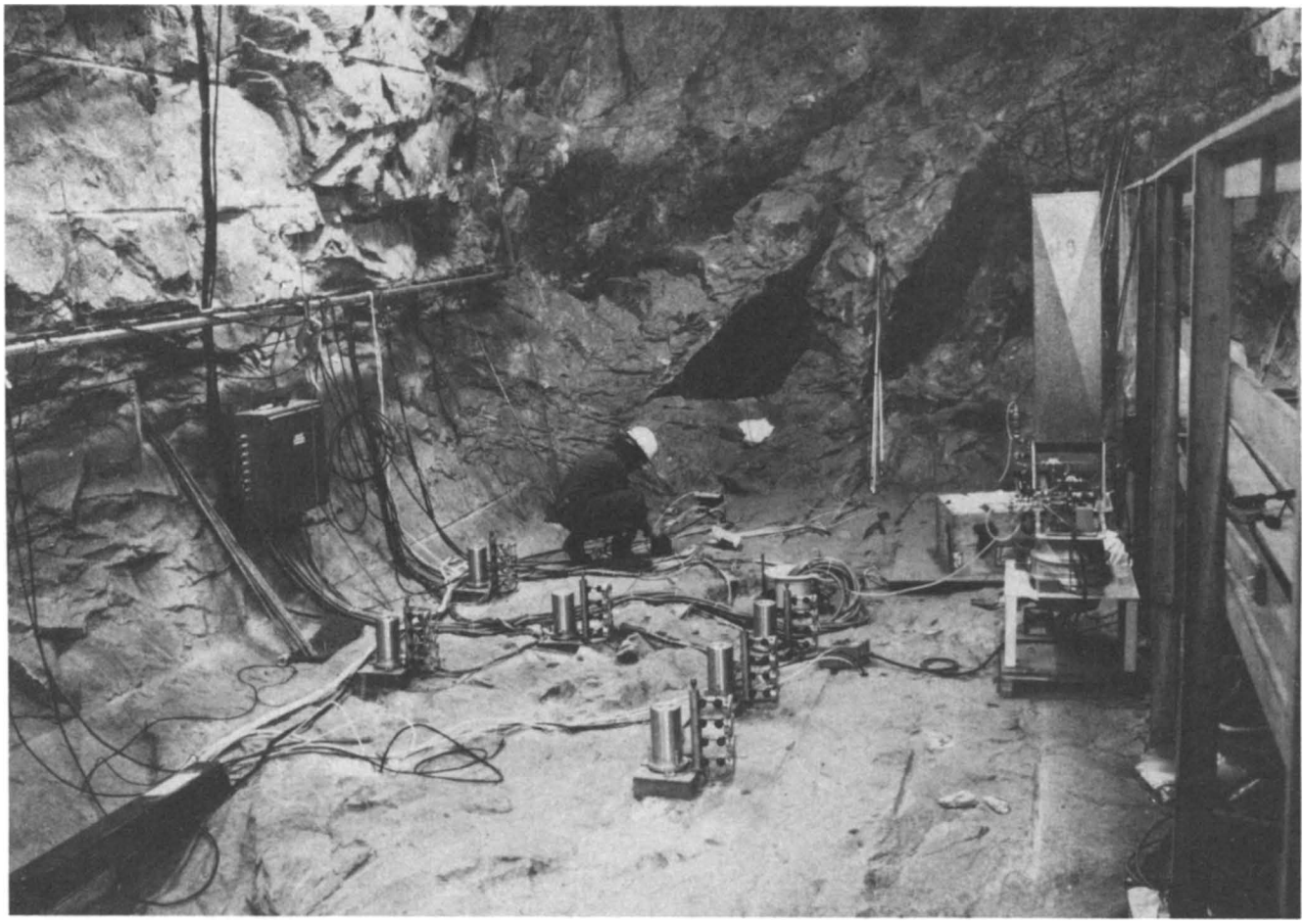

FIG. 1. The end of the experimental drift where the cross-hole ultrasonic experiment was conducted. Shown in the photograph is the heater (right lower center) and the collars of the extensometers placed in a number of vertical boreholes. Also shown are the smooth walls and floor from careful blasting.

apparent homogeneity and relative lack of foliation. The full extent of fracturing and brecciation becomes apparent only in thin sections. Most fractures are completely filled, but openings can be seen in some thin sections, as shown in Figure 3. A sample of granite from a pluton 1 km from the Stripa site in Figure 4 shows good contact between grains. In the Stripa thin section the quartz grains are completely surrounded by fracture infilling material, which in this case is sericite, but often calcite or chlorite is found. Even in relatively unfractured Stripa samples, discontinuous cracks are common within primary grains and along grain boundaries.

In the H9 heater area, 224 m of oriented core were recovered from 20 boreholes with diameters of 56 or 76 mm. From all this core some 4 000 open and closed fractures were logged, about half of them in cores which were oriented. Detailed fracture data and analyses can be found in Paulsson et al. (1981). The average distance between these fractures was 0.12 m. Plotted fracture poles form two primary clusters, at N30E dipping 30W and at N10E dipping 65W as seen in Figure 5 on a Schmidt lower hemisphere net. A total of 1 885 open and closed fractures from oriented core from both vertical and horizontal boreholes is shown. The majority of the fractures are filled with chlorite, but epidote also occurs as a fracture-filling mineral, especially at the end of the drift where the cross-hole experiments were conducted. Fractures filled with calcite, which probably is the youngest fracture set and is the most likely conduit for water, also occur frequently. The calcite fractures were also the weakest fractures. Only 10 percent of the calcite fractures remained intact during core retrieval as compared with 70 percent of the fractures filled with epidote. Despite careful logging it proved very difficult to correlate one particular fracture in a borehole with a fracture in a neighboring borehole only 2 to 4 m away, even though the surface expressions of most fractures show they are planar (see Figure 6 which shows the fractures in the heater midplane). The only features recognized in all boreholes were the major features such as pegmatite dikes and epidote fractures and faults.

THERMAL AND THERMOMECHANICAL HISTORY

The Stripa heater experiment was closely monitored by thermocouples, stress gauges, and extensometers. The water inflow to the instrument holes was recorded as water was removed during the course of the experiment. Dewatering of the rock

Table 1. Composition of Stripa red quartz monzonite.

Mineral	Volume %
Quartz	37.1
Partly sericitised plagioclase	32.0
Microcline	22.2
Muscovite	7.4
Chlorite	1.3
Accessory minerals	—

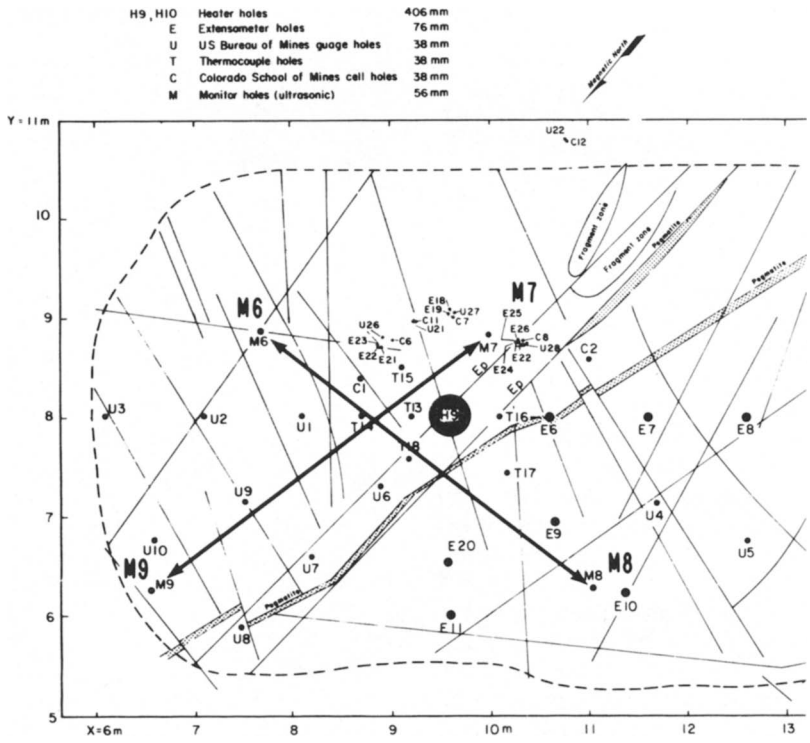

FIG. 2. Plan of the drift floor and the various boreholes for the H9 heater experiment. M6, M7, M8, and M9 used in the cross-hole study are accented. Dashed line is the drift wall, solid lines show mapped fractures and dikes at the drift floor. The two heavy lines which cross represent the two main cross-sections M8-M6 and M7-M9.

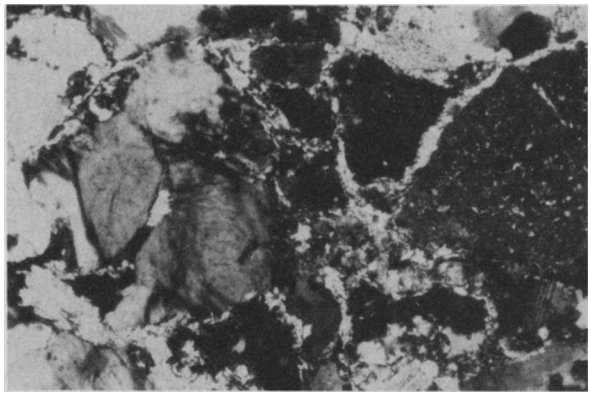

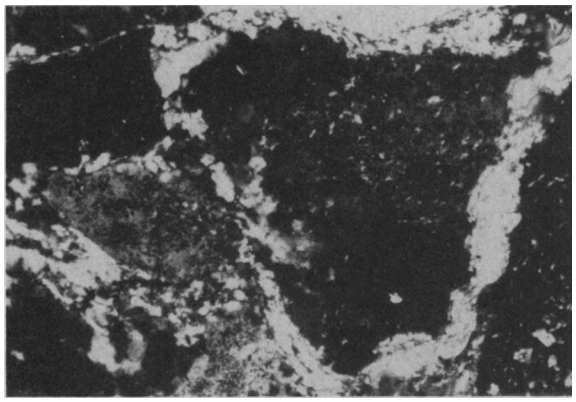

FIG. 3. Thin section from the full-scale drift in the Stripa pluton. The upper photograph presents a 1.32-mm wide view, and the lower section is 0.66 mm across. The extensive microfracturing between each grain is apparent.

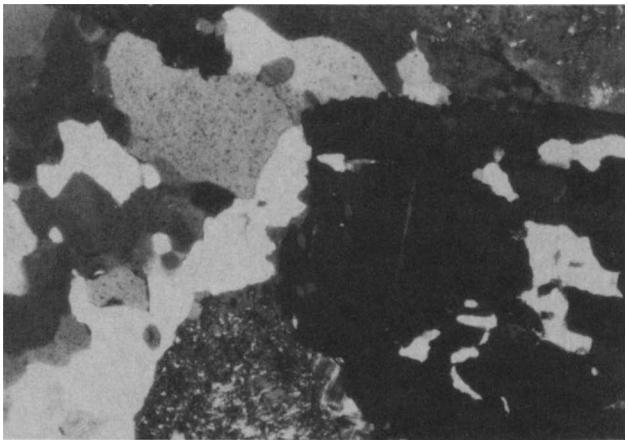

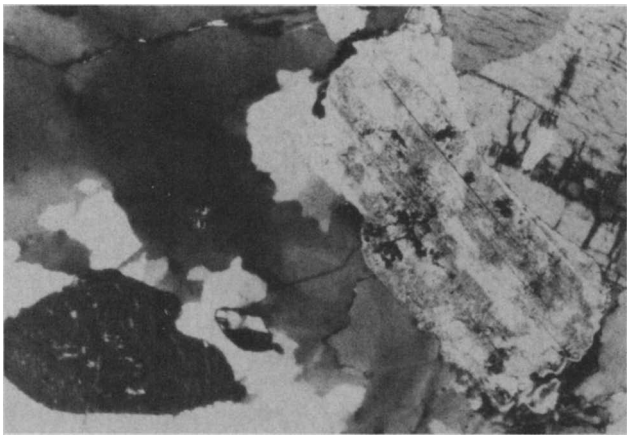

FIG. 4. Thin section from a granitic pluton adjacent to the Stripa mine. The upper photograph presents a 1.32 mm wide view and the lower section is 0.66 mm across. The microfracturing which was so abundant in the Stripa pluton is not found in this granite.

mass began prior to turn-on of heater H9 and spanned the 398-day heater operation.

There were two related active processes occurring in the rock mass: thermal expansion and pore water expulsion. Both phenomena changed the properties of the rock surrounding the heater hole and the instrument holes. The thermal changes in a rock mass due to heating are fairly well understood, and theoretical calculations of the temperatures proved very close to the measured values. Stresses and displacements calculated by Chan et al. (1980) for a crack-free medium prior to the experiment were higher than the observed stresses and displacements, because the bulk of the thermal expansion was apparently absorbed by abundant fracturing present in the quartz monzonite. No predictions were made on the effects of dewatering. It is shown later that expulsion of the pore fluid has a profound effect on wave propagation around the heater and deeper in the rock mass.

The theoretical temperature fields around the Stripa heaters were presented in Chan et al. (1978). There are 15 thermocouples in the heater midplane within a radius of 5 m and seven within 1 m from heater H9 where the thermal gradient is steepest. The measured temperatures followed calculated predictions closely in most cases. Figure 7 shows the measured and calculated temperatures in the heater midplane at four different radial distances from the heater. The four thermocouples are 0.40, 0.89, 1.50, and 2.99 m from the center of the heater, respectively. The heater radius of 0.2 m should be subtracted to obtain the distance from the heater wall to the thermocouple. Figure 8 shows the average temperatures in the four seismic lines in the heater midplane. Note the rapid increase of the mean temperature when the heater was turned on, and the equally rapid decrease when the heater was turned off.

There were approximately 75 thermocouples in the rock mass within a radius of 4.0 m from the H9 heater hole. Resulting data provided the temperature distribution in the cross-sections A–F. Figures 9 and 10 show temperature distributions in section E(M8-M6) and F(M7-M9) for the last day of operation of the 3.6 kW heater. At the top of each figure is the position of the cross-section relative to the heater hole.

Thin sections of the Stripa granite show abundant micro-

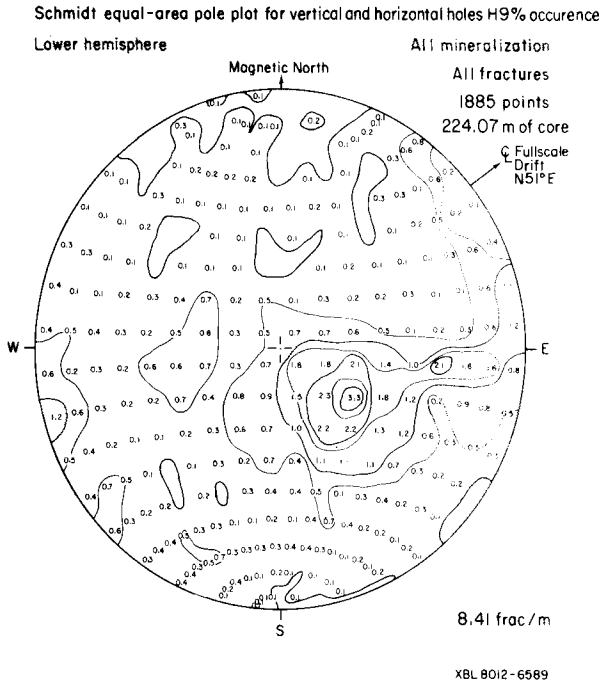

FIG. 5. Pole plots on a Schmidt equal-area stereo net for all the fractures recorded in oriented core in the H9 heater experiment.

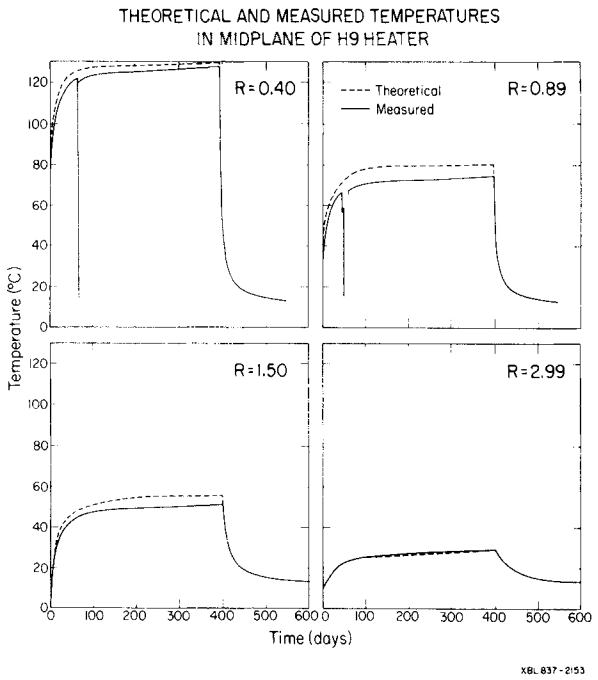

FIG. 7. Temperature record from four thermocouples in the H9 heater midplane at 0.40, 0.89, 1.50; and 2.99 m from the center of the 0.2 m diameter heater, respectively. The temperatures are shown for the period from turn-on of heater H9 until day 600. The heater was turned off on day 398.

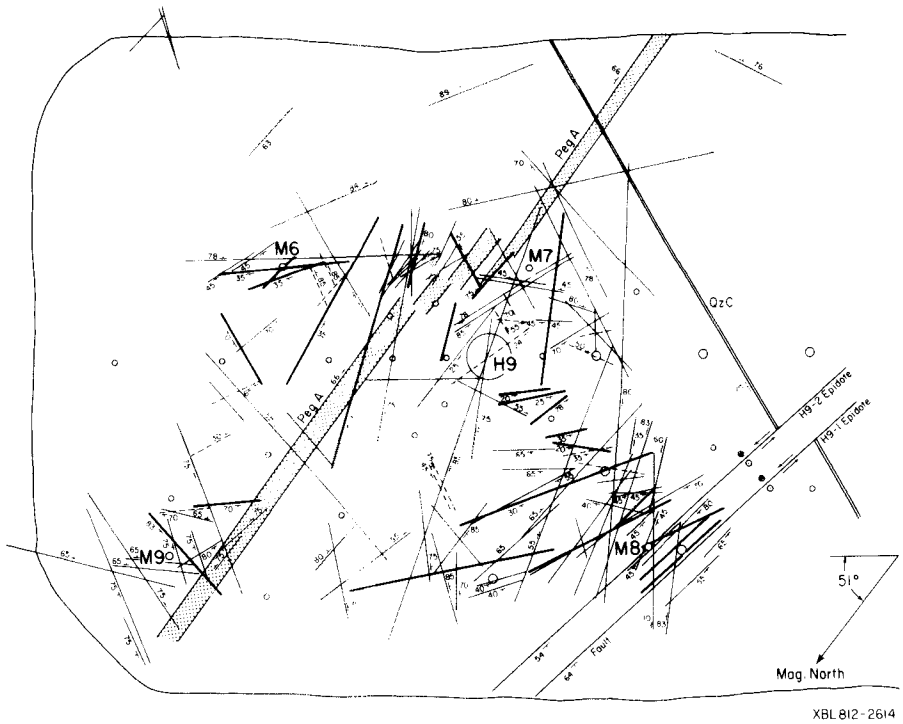

FIG. 6. Fracture map of the H9 heater midplane showing faults (H9-1, 2), pegmatite dikes, and fractures. The map was constructed from directional fracture data logged in core and projected on the midplane.

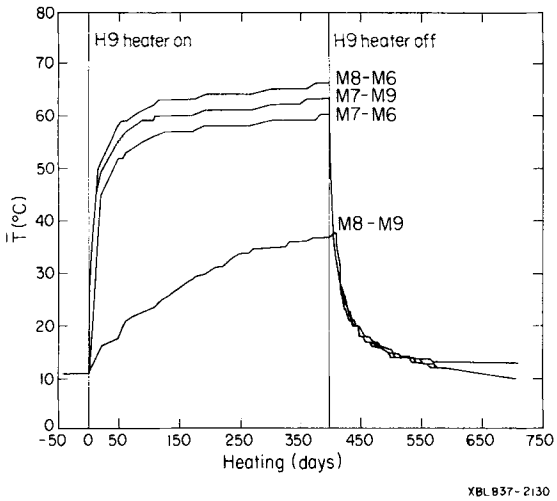

FIG. 8. Average temperatures over the four monitor lines from day −40 to day 710. These mean temperatures were obtained by projecting the radial temperature function from the heater onto 100 equally spaced points along lines connecting the M boreholes. This was done for the 103 days over which data were collected in the heater midplane.

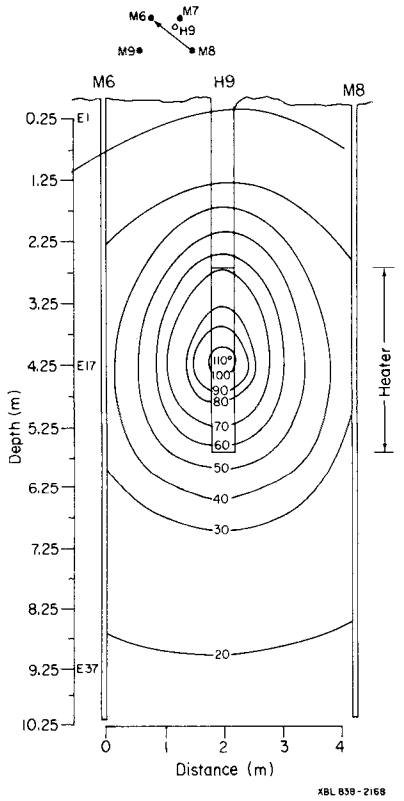

FIG. 9. Temperature distribution in cross-section M8-M6 on day 398 after heater H9 turn-on.

fractures throughout the rock. As the rock mass is heated, thermal expansion increases the normal stress on fractures and tends generally to close them, working against any pore fluids. This phenomenon is most pronounced in the zone of highest stress adjacent to the heater, and as one moves nearer the heater, more closed fractures are expected.

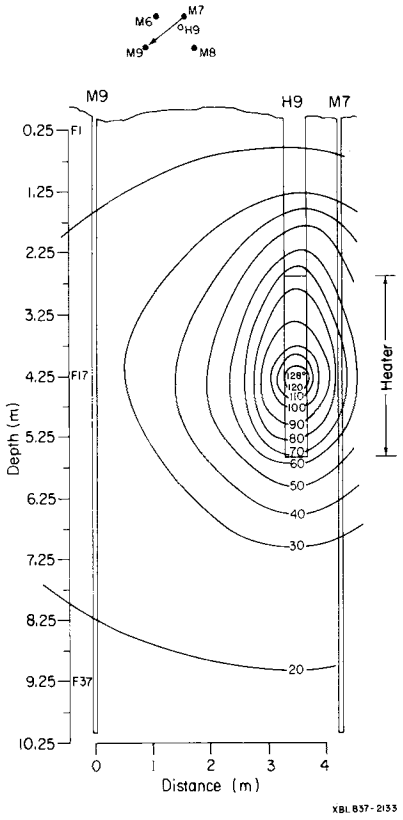

FIG. 10. Temperature distribution in cross-section M7-M9 on day 398 after heater H9 turn-on.

Field stresses

Directions and magnitudes of field stresses, i.e., those stresses existing in the rock prior to excavation, plus induced stresses produced by excavation can be estimated by measurements and from geologic information. Geologic phenomena which can provide an indication of the stress directions in the area of heater H9 are the fault directions and the pegmatite dikes. Figure 11 shows the principal stress directions obtained from measurements made in surface and mine boreholes, along with the directions of faults in the H9 and H10 areas. The polar representation of pegmatite dikes A and B are also shown. Faults H9-1 and H9-2 are reverse faults with principal compressive stress σ_1 horizontal and perpendicular to the strike of the faults (Jaeger and Cook, 1979) and vertical minimum principal stress σ_3. In Figure 11 the polar representations of the faults fall close to the line M8-M6. Paulsson (1983) showed that there is also a strike-slip component in the faulting, which is indicative of horizontal principal compressive stress at some angle to the strike direction. The steeply dipping pegmatite dike indicates a minimum principal stress direction perpendicular to the pegmatite plane at the time of intrusion of the dike. The stresses may have changed from the time of the faulting and instrusion of the pegmatite. However, measurements by Doe et al. (1981) and Doe (1982) with both overcoring and hydrofracturing techniques produced data which (although showing considerable scatter) are fairly close to the stresses inferred

above, with a maximum compressive stress close to horizontal but directed in a northwesterly direction. Figure 11 shows results from Carlsson (1978) and Doe et al. (1981) with the fault and dike data. The induced stresses produced by the excavation are expected to decrease the component of stress radial to the drift, increase that component tangential to it, and have little effect on the axial component.

Dewatering

Dewatering of the rock mass, described in detail in Nelson et al. (1981), began after rather large quantities of water were found being expelled into the boreholes. In order to prevent boiling and convection in the heater holes and convection in the thermocouple holes, dewatering [by pumping the 18 T, U, and C boreholes (Figure 2)] began 41 days before heater turn-on and continued through day 545. The amount of water removed was recorded each day. Figure 12, from Nelson et al. (1981), shows inflow for some of the dewatered boreholes in the H9 area.

Upon turn-on of all four heater experiments there was an increase of water inflow to the boreholes. The wall temperature of borehole H9 reached a maximum of approximately 300° C. Around heater H9 a very sharp temperature gradient existed, with high values only near the heater (see Figures 9 and 10). Five liters of water flowed into the holes after heater H9 was turned on. Nelson et al. (1981) showed that a porosity change of 0.1 percent with 0.1 mm fractures spaced at 0.1 m can produce this volume of water. The depth at which the water entered the boreholes is not known. Flows in boreholes T17 and T18, at distances of 0.8 m and 0.6 m from the heater center, respectively (shown in Figure 12) decreased to zero after 100 days. Nelson et al. (1981) observed that the boreholes in the end of the drift (the most distant from the heater) had a much higher inflow during the course of the experiment. They concluded by studying the water inflow data that permeability increased with radial distance from the heater H10 hole.

EXPERIMENTAL PROCEDURES AND DATA PROCESSING

Drilling, surveying, and dewatering

Seismic measurements were made between four drained, vertical boreholes of 10 m depth located in the vicinity of the vertical heater borehole H9 as shown in Figure 13. The primary M8-M6 and M7-M9 sections are almost perpendicular and both pass close to the heater. The boreholes were surveyed for location at the collar, in the middle, and at the bottom of the

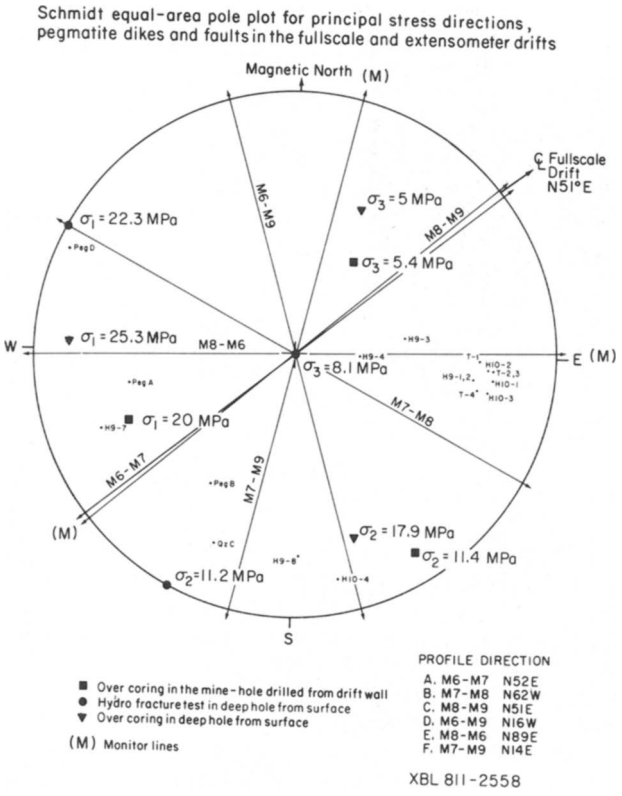

FIG. 11. Schmidt equal-area plot for various principal stress directions. Poles of the pegmatite dikes and faults mapped in other holes in the H9 heater area are also shown, along with the directions of the six seismic cross-sections. The stress data are from Carlsson (1978) and Doe (1981).

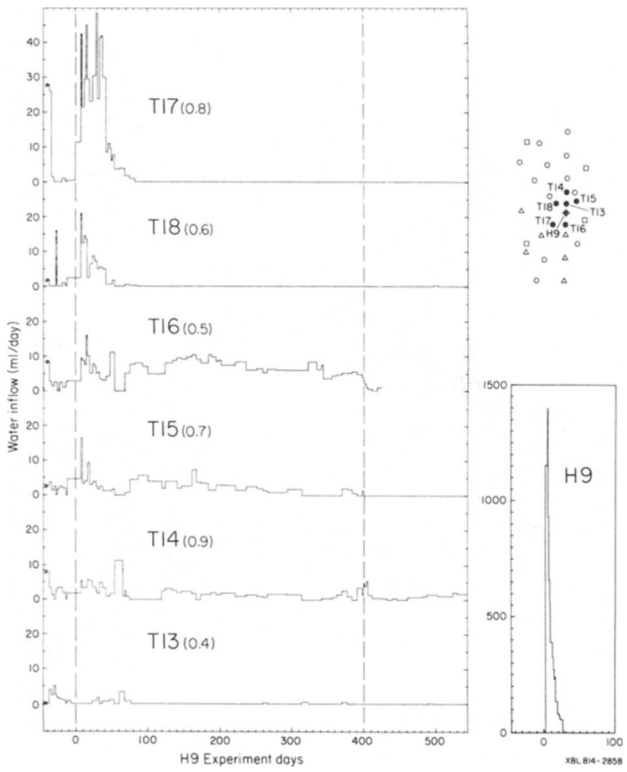

FIG. 12. Water inflow record for H9 and associated T holes. The increase in inflow of water is seen in most of the boreholes. The inflow of water in the H9 heater borehole indicates fracture closure after turn-on of the heater. Also shown is a map with the position of the boreholes in this figure (after Nelson et al., 1981).

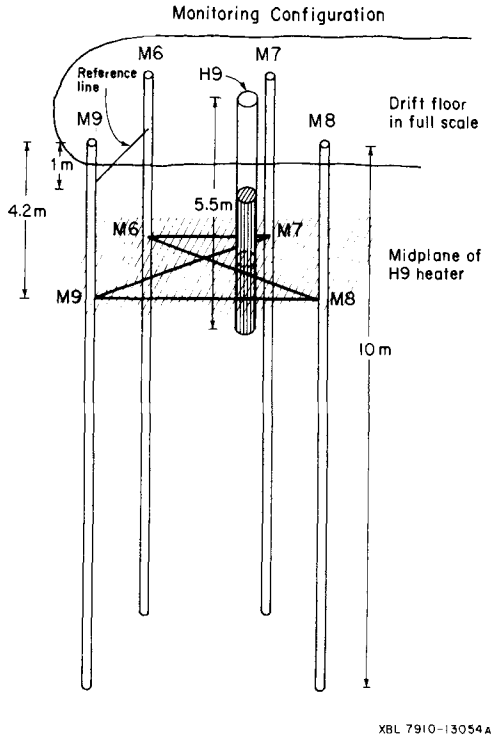

FIG. 13. Borehole system showing heater borehole, monitor boreholes, the reference line, and the monitor lines.

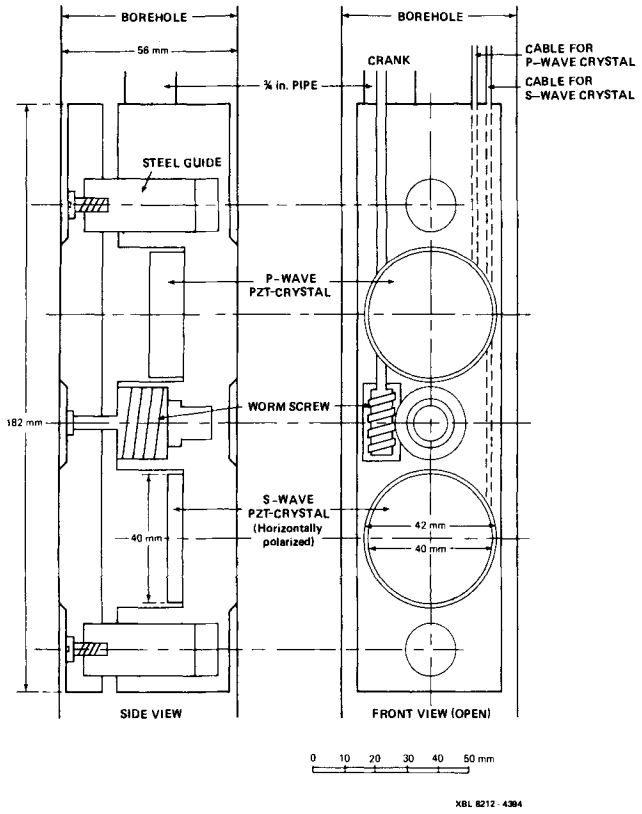

FIG. 14. Detailed diagram of a cross-hole transducer. The only differences between the transmitter and the receiver are the cables and that the receiver is equipped with a line-matching transformer.

holes with an accuracy of ± 0.5 mm in the X, Y, and Z directions. Forty positions for seismic transmission and reception were spaced at 0.25 m along the length of each M borehole. The total position accuracy, ± 1 mm, represents 0.025 percent for the 4.2 m M6-M8 line. The positions of the transducers were easily reoccupied over the duration of the experiment. Small amounts of water continually seeped into the four boreholes, but they were blown out regularly to dry them.

Transducers and data acquisition system

Transducers were mechanically jacked to the borehole wall by a worm-screw operated by a long rod. The transducers are constructed as two semicylinders with the transducers and the jack in the larger of the two parts, as shown in Figure 14. The two parts of the transducer were pushed apart against the walls of the borehole. Orientation within the boreholes was repeatable to about ± 5 degrees. The transducer housings are constructed of aluminum, which has a similar acoustic impedance to that of the granitic rock. The crystals used to generate and receive the acoustic signals were made from PZT-5 (lead-zirconate-titanate).

A high-voltage pulse generator excites the transmitting transducers and generates a coincident synchronizing pulse as a trigger for transmission time measurements on the oscilloscope and the tape recordings. The pulse repetition rate of 30 ms allowed time for the signal to dissipate between pulses. Separate P- and S-wave transducers of nominal 220 kHz resonant frequency were used as transmitters and receivers. Instrument delays of 6.2 μs for the P-wave pulses and 11.3 μs for the S-wave pulses were obtained by clamping the transmitter and receiver together and recording the arrival times.

The received P- and S-wave signals were displayed on an oscilloscope screen and recorded in analog form on an instrumentation direct-record tape recorder for later analysis in the laboratory. Typical oscilloscope traces for the 2.8 m reference line are illustrated in Figure 15. Both P- and S-wave arrivals are sharp and may be picked precisely. The resolution of the arrival time is estimated to ± 0.014 percent of a total traveltime of 0.700 ms. Together with the ± 1 mm uncertainty in the coordinates for each data point one obtains a total accuracy of better than ± 0.05 percent in the calculated velocities. In the case of M8-M6 where the P-wave velocity was approximately 6 000 m/s, this results in a velocity resolution of ± 3 m/s.

Data

Data were gathered in three different modes of sampling. In monitoring mode, arrival times for the four lines in the heater midplane were sampled on a regular basis. In survey mode, the six cross-sections were sampled several times in the course of the experiment to obtain two-dimensional data on velocity variations. The third mode (performed only a few times) consisted of a downhole velocity survey.

In the monitoring mode one transmitter was placed in borehole M8 and directed toward borehole M6, while a second transmitter was placed in borehole M7 and directed toward borehole M9 (see Figure 13). While M8-M6 and M7-M9 were the main monitoring lines, data were also collected for lines M7-M6 and M8-M9, although in so doing the transducers were not turned to face each other. Thus in effect both the transmit-

ter and the receiver were directed approximately 45 degrees from the line connecting them. Transmission time was not affected, but the waveforms were altered considerably. There were approximately 100 recordings during the experiment of both *P*- and *S*-waves from each of the four monitoring lines. Because of time constraints before the turn-on of heater H9, only a short run of preheating data was recorded. Also, because of operational problems, only a limited number of data were collected during the initial phase of the heater experiment. During the "steady state" part of the heater experiment, seismic data were collected every other week. Finally, when heater H9 was turned off, data were collected twice a day for two weeks in the heater midplane.

Data were collected most frequently both in space and in time for the profiles M8-M6 and M7-M9—ten surveys were run during the course of the experiment for each of them. For the remaining four profiles, five surveys were performed with less dense vertical sampling. The crosshole surveys were designed to investigate any correlation of velocities or attenuation with geologic features and to map response of the rock during the course of the experiment as a function of vertical and horizontal distance from the heater.

Downhole surveys were performed in May, 1978, before the heaters had been turned on and before dewatering of the rock mass had begun, and in July, 1980, immediately after dewatering of the rock around heater H9 had stopped.

A reference line (shown in Figure 13) was chosen between boreholes M6 and M9 at a depth of 1 m from the floor of the drift; the line is 3.2 m above the heater midplane. Relatively small perturbations of traveltimes and wave characteristics were expected along the reference line when heater H9 was turned on. Indeed, the velocity there changed only about 20 m/s (0.3 percent) over the 750 days. The amplitude spectra, however, changed considerably in the reference line, with associated *Q*-values for the *P*-waves changing from 14 to 25 (80 percent), of the same order as the changes seen in the heater midplane. The stable arrival times of the waveforms in the reference line proved to be very helpful for detecting bad transducers or other problems.

For convenience in processing, some 20 000 parameters and 4 000 waveforms were archived by the analysis system. The traveltimes with the instrument delay subtracted were then used with the path distances to obtain the apparent mean *P*- and *S*-wave velocities between boreholes. We assumed that the

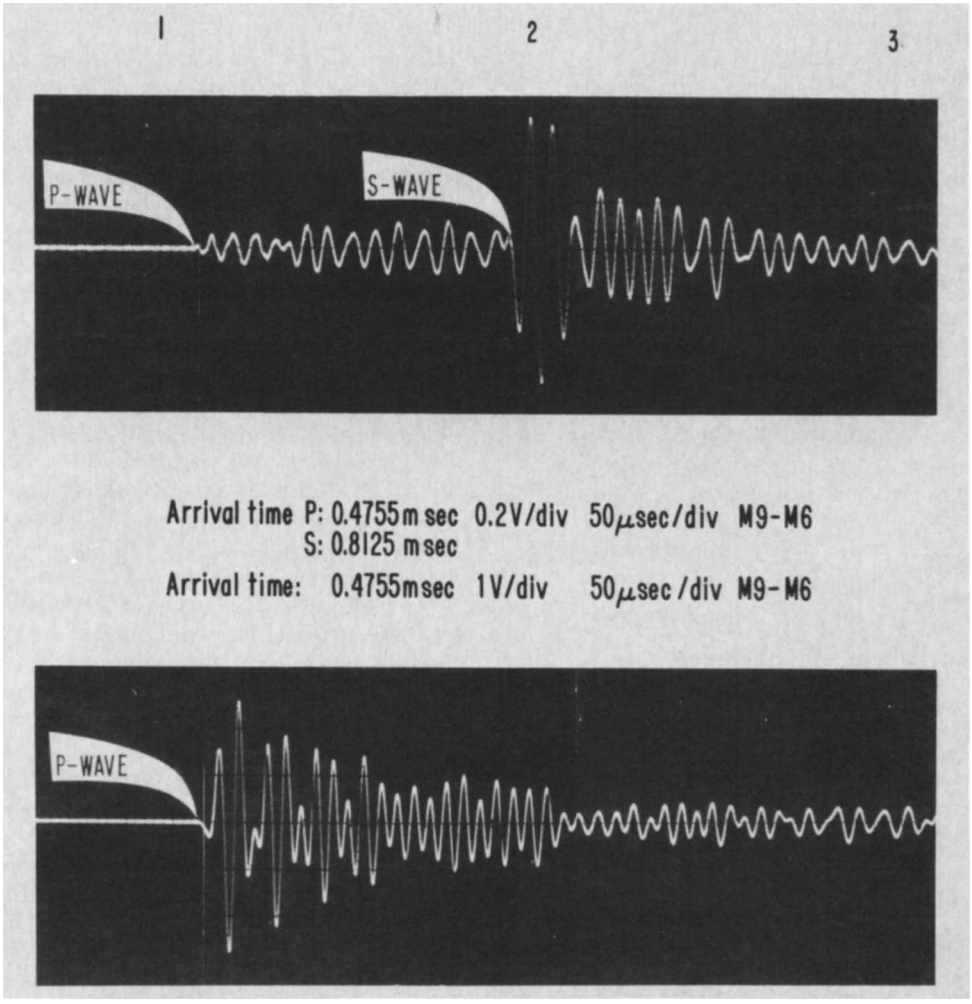

FIG. 15. Oscilloscope traces of received ultrasonic signals in the reference line (M9-M6). Upper trace is for the *S*-wave source and receiver, and the lower trace for the *P*-wave source and receiver.

waves travel along straight line paths between the boreholes. Velocity anisotropy is not considered sufficient to cause any noticeable difference in travel path. The heater region represented an initial low-velocity zone which disappeared upon heating. Raypaths would thus have curved away from the heater area initially and straightened upon heating, so that the 2 to 4 percent changes seen in traveltimes represent minimum estimates.

Analog signals recorded on tape in the field were played back in the laboratory and digitized utilizing a Tektronix digital processing oscilloscope (DPO). The DPO is connected to a DEC 11-34 computer, and the software and data are stored on discs via two floppy disc drives. Q-value changes were determined from ratios of the Fourier amplitude spectra to a reference spectrum as described by McDonal et al. (1958), Tullos and Reid (1969), and Toksöz et al. (1979). Signals were windowed with a 70 μs half-cosine window and normalized to unity peak amplitude prior to the Fourier transformation.

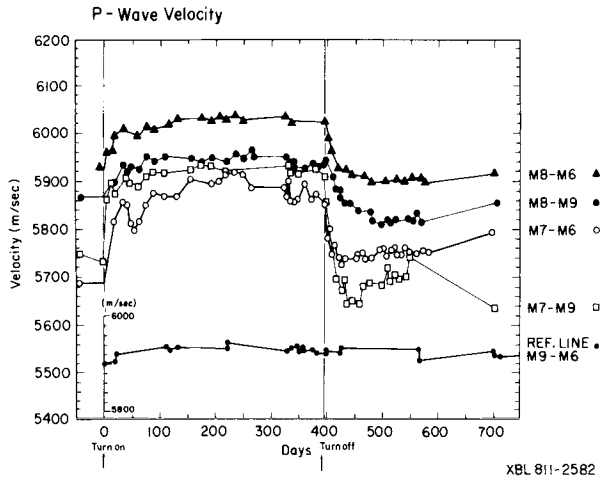

FIG. 16. P-wave velocities in the four monitoring lines and the reference line. For clarity, not all data points are shown.

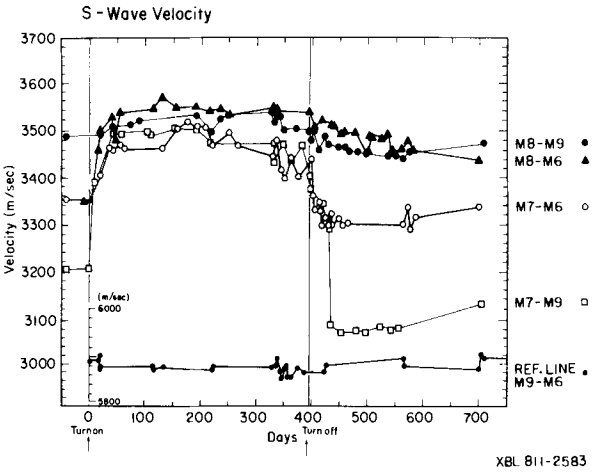

FIG. 17. S-wave velocities in the four monitoring lines and the reference line. For clarity, not all data points are shown.

The wave amplitudes varied as a function of the smoothness of the borehole wall, so the field system used did not provide absolute amplitude control of the signals. The lack of absolute amplitude alone did not alter the slope of the spectral ratio used in the Q-value calculation, because the borehole wall coupling changes did not produce a frequency-dependent effect.

OBSERVATIONS

The cross-hole study involved three modes of data collection: the monitor mode, the survey mode, and the downhole mode. One objective was to investigate the utility of cross-hole velocity measurements used to identify heterogeneities in the rock, including fracture zones. A second objective was to investigate the sensitivity of measurements of velocities and attenuation of elastic waves used to study physical properties of the medium as they changed over the course of the experiment.

Traveltime changes

Monitor data.—In the monitoring mode the transmitters were placed at the heater midplane depth in boreholes M7 and M8 with the receivers in boreholes M9 and M6. P- and S-wave data for the four lines sampled in the 750-day experiment are shown in Figures 16 and 17.

Immediately following turn-on of heater H9, sharp increases of the P-wave velocities were observed. Velocities increased more slowly until about day 150 after heater turn-on, and then remained fairly constant until the heater was turned off on day 398. The velocity increase in the heater midplane varied between 60 and 200 m/s for the four monitor lines. During the initial stages of heating, at approximately day 30, the P-wave velocity reversed for about 50 days.

After heater H9 was turned off, traveltimes were closely monitored. Velocities decreased sharply to values below those recorded before the heater was turned on. Over line M7-M9 the effect is particularly noticeable. Note that this path passed closest to the heater: the shortest distance between the heater borehole wall and the M7-M9 cross-section is 0.2 m. Over all four lines the velocity passed through a minimum between 50 to 200 days after the heater turn-off, and from then on the velocity increased slightly, probably due to resaturation.

The S-wave velocities in the four monitor lines and the reference line are given in Figure 17. S-wave velocities increased when the heater was turned on and, when the heater was turned off, the velocities decreased on all four lines. In two of the lines, M8-M6 and M8-M9, the change was small and the S-wave velocities remained elevated in these two lines after the heater experiment. After dewatering ceased, the S-wave velocity gradually increased in three of the four lines.

Survey data.—The first vertical profile surveys were performed for P-waves on all six sections 44 days before the heater was turned on and 3 days before dewatering of the rock mass began. Therefore, the first surveys measured the rock mass before any appreciable volume of water had been drawn from it. The physical properties controlling the velocities are the degree of fracturing which affects the stiffness of the rock, and the orientation of the profile under consideration relative to the principal stresses. Figure 11 shows the directions of the six cross-sections with the major faults, dikes, and principal stresses.

Figures 18 and 19 show the velocity data for surveys in two main, diagonal sections that pass near the heater borehole. The six preheating surveys showed vertical velocity variations, with correlation between the size of the velocity anomaly and proximity of the cross-section to heater H9.

When heater H9 was turned on, the velocities increased in all six cross-sections at depths extending more than 4 m below the bottom of the heater. Cross-section M8-M6 (shown in Figure 18) offers an interesting study of *P*-wave velocities as a function of changes in temperature. The velocities were observed to increase in four surveys performed while heater H9 was turned on, during days 20, 111, 118, and 341. The difference between day 118 and 341 is small but noticeable. The first survey after heater turn-off on day 420, 22 days after the turn-off of heater H9, shows how sharply the velocities decrease. This behavior mirrors the very rapid decrease in temperature observed around heater H9, shown in Figures 7 and 8. The last survey, on day 704, shows a residual low-velocity zone between levels 9 and 17, with the largest *P*-wave velocity change at line 13 from the drift floor (lines or measurement levels, are spaced at 0.25 m intervals vertically). The maximum temperature adjacent to the heaters was naturally at the midplane (line 17), but it is notable that the largest permanent velocity change (260 m/s) occurred in a zone with calcite-filled fractures some 0.5 m above the midplane at the comparatively low temperature of 60° C.

Cross-section M7-M9 (Figure 19) is closest to heater H9, only 0.2 m from the H9 borehole wall at the closest point, where the temperature as shown in Figure 10 reached almost 130° C. Four surveys, on days 13, 20, 111, and 349, were performed over this cross-section during the period the heater was turned on. Results are similar to those for section M8-M6, with the greatest velocity change of 290 m/s seen on day 349. When the heater was turned off, the velocities decreased more rapidly in this section than the other sections surveyed, reaching a very low value at depth F16 (Figure 19) before recovering. The last survey, on day 707, shows that between F6 and F19 in Figure 19 the postheating velocities are found to be lower than the preheating values. In Figures 20 and 21 the waveforms from selected surveys are shown for both M8-M6 and M7-M9 sections, illustrating the contrast between traveltimes when the heater is on and after it has been turned off.

There is some uncertainty as to the magnitude of the stresses around heater H9 because of (1) the unknown temperature dependence of moduli and thermal expansion on temperature, and (2) a lack of knowledge of the constitutive law when stress can be accommodated in part by slip on fractures. Temperatures are easier to predict, and it is temperature change which drives the process by causing the expansion of the rock and subsequent narrowing of cracks. It seems more fundamental then to relate change of velocity with change in temperature. In Figure 22 the velocity changes from day 0 to day 340 are plotted as a function of the change in mean path temperature for a series of depth points for cross-sections M8-M6 and M7-M9. Regression analyses of the resulting plots for the four cross-sections are given in Table 2. The coefficients vary from 2 to 4, with the smallest value seen for M8-M6, oriented close to the direction of maximum compressive stress (see Figure 11). Note that the initial velocities and elevated values are lowest for M7-M6, in the axial direction of the drift.

Fehler (1981) reported a decrease in the *P*-wave velocity of 1.07 km/s for a decrease in temperature of 100°C (11 m/s/°C) which may be compared with the results in Table 2 for a maximum change in temperature of about 60°C. Fehler concluded that the compressional velocity changes linearly with temperature. This agrees with our results. Differences in confining stress and fracturing between in-situ and laboratory conditions, as well as natural differences between the two granitic rocks, are likely causes for the differing slope values.

It is possible to estimate the change in fracture porosity in the granite from the observed changes in *P*-wave velocity and an intrinsic *P*-wave velocity calculated from the modal composition of the rock. The total fracture porosity so determined in cross-section M8-M6 is 1.45 percent, implying that the part of the 4.18 m path occupied by water is 60.8 mm. Using a coefficient of thermal expansion of water of 1.7×10^{-4}/°C, the average temperature increase of 56°C yields a thermal expansion of the water in the line of the section of 0.6 mm, compared with the 2.34 mm thermal expansion calculated for the rock.

Assuming that the change in velocity is dependent only on the change in porosity, the changes in porosities estimated for lines M8-M6 and M7-M9 are 0.23 and 0.16 percent, respectively, in general agreement with the mean total effective connected fracture porosity of 0.1 percent suggested by Gale et al. (1982) for the Stripa site. The change in the fracture porosity in the M8-M6 and M7-M9 lines is approximately 0.2 percent. If the volume around the H9 area affected by dewatering is estimated at $5 \times 5 \times 10$ m, one obtains a change in fracture volume of 0.5 m^3. The total amount of water recovered was 0.4 m^3 which is close to the change in the calculated change in the fracture volume. While these results are based upon a number of intertwined assumptions, the values are supported by independent studies, and they provide a coherent, self-consistent description of the coupled thermomechanical-hydrological processes in operation around the heated borehole.

Downhole data.—The limited downhole work performed is important in that it provides the velocities in the immediate vicinity of the monitor boreholes. Figures 23 and 24 (from King and Paulsson, 1982) show the compressional wave velocities for the four boreholes. The lower velocities are found in boreholes closest to the heater. The velocities are generally low near the drift floor, probably a result of mining damage. In borehole M9 there is a low-velocity zone at depths between 4 and 5 m. There is a cluster of calcite fractures at this level which may be responsible for the low velocities. Velocities measured downhole in the vertical direction are generally 10 percent lower than those observed cross-hole in the horizontal direction. This probably occurs because the minimum principal stress occurs in the direction radial to the drift and therefore almost parallel to the vertical boreholes. Also, any damage by drilling will preferentially affect the downhole measurements. In any event, the patterns of velocity increase in the heated condition are similar for either set of measurements.

Attenuation changes

Changes in medium attenuation, represented by Q the intrinsic quality factor for the path material, were calculated using a spectral-ratio technique for the set of *P*-waveforms from which the velocities were obtained. The amplitude spectrum for a plane wave propagating in a homogeneous medium can be written as

$$A(x, t) = A_0 x^{-n} e^{i(kx - \omega t)}, \quad (1)$$

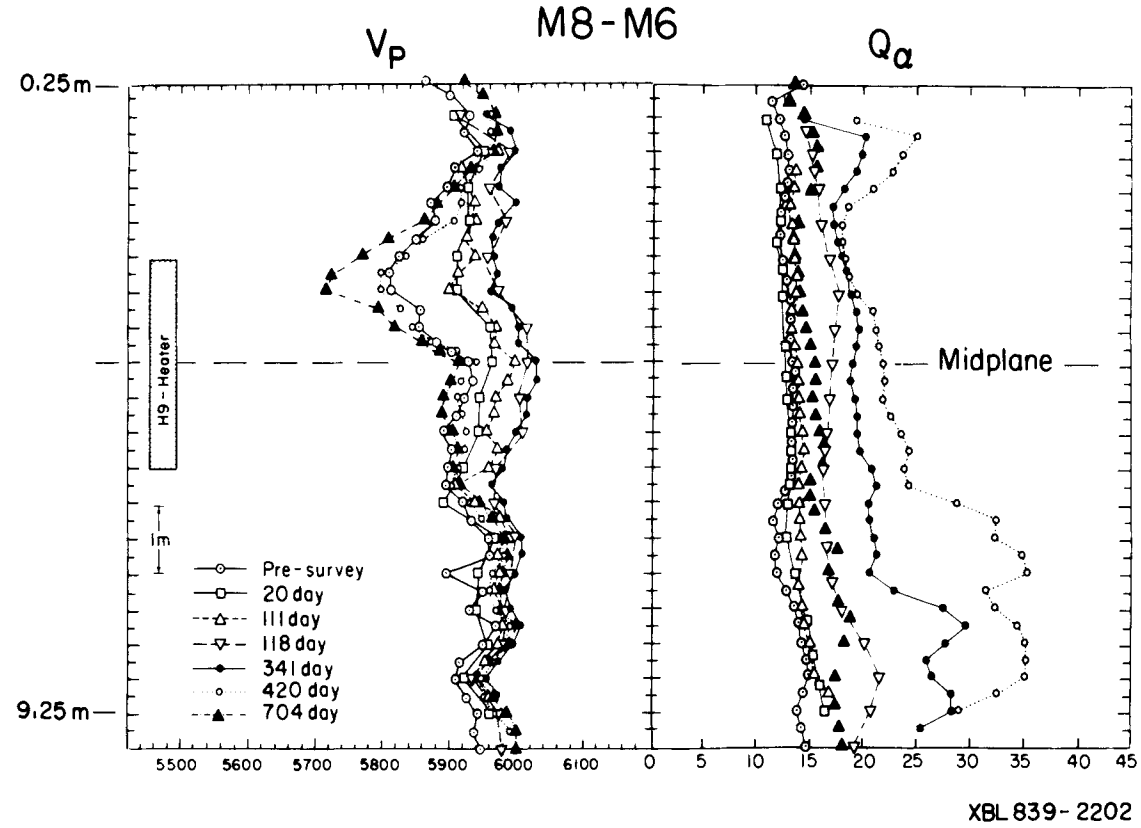

FIG. 18. *P*-wave velocities and Q_α in cross-section M8-M6 for seven surveys at days −44(1), −7(2), 20(3), 111(4), 118(5), 341(6), 420(7), and 704(8). The maximum line number represents 9.75 m below the drift floor.

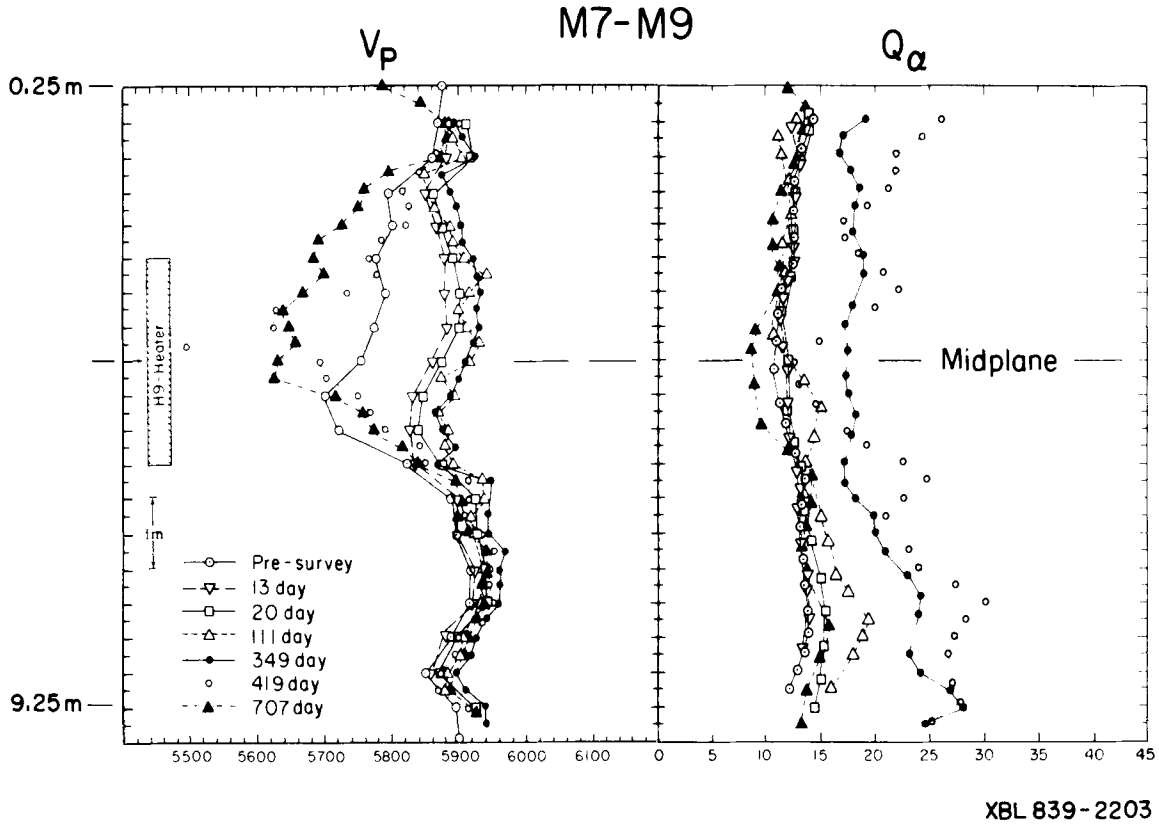

FIG. 19. *P*-wave velocities and Q_α in cross-section M7-M9 for seven surveys at days −43(1), 0(2), 13(3), 20(4), 111(5), 349(6), 419(7), and 707(8).

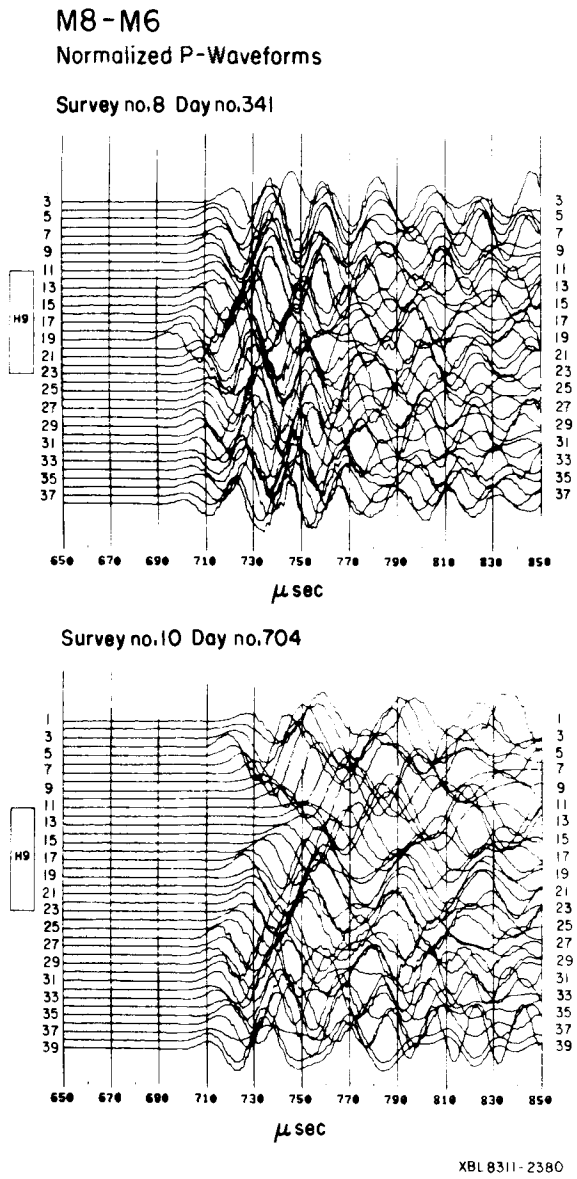

FIG. 20. Waveforms from cross-section M8-M6, for survey 8 on day 341 and survey 10 on day 704. The 3 m long H9 heater is scaled correctly with respect to the cross-hole data lines.

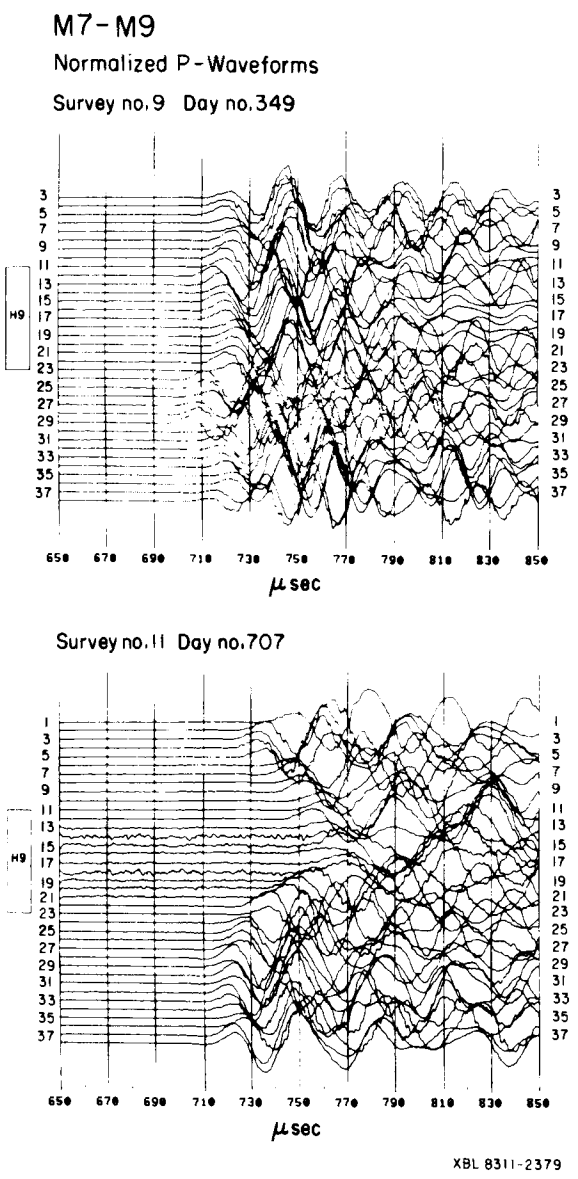

FIG. 21. Waveforms from cross-section M7-M9, for survey 9 on day 349 and survey 11 on day 707.

Table 2. Temperature-velocity function in four vertical cross-sections.

Line	Correlation	Intercept	Standard error of intercept	Regress. coeff. (slope) (m/s/°C)	Standard error of reg. coeff.	$\overline{V_p}$ at non-anomaly zones	$V_{p(\max)}$
M7-M6(A)	0.77	17.9	38.8	3.05	0.63	5 872	5 938
M7-M8(B)	0.81	5.6	46.3	4.00	0.71	5 951	5 979
M8-M6(E)	0.80	22.2	24.1	1.95	0.37	5 955	5 970
M7-M9(F)	0.93	7.7	19.7	3.26	0.31	5 907	5 932

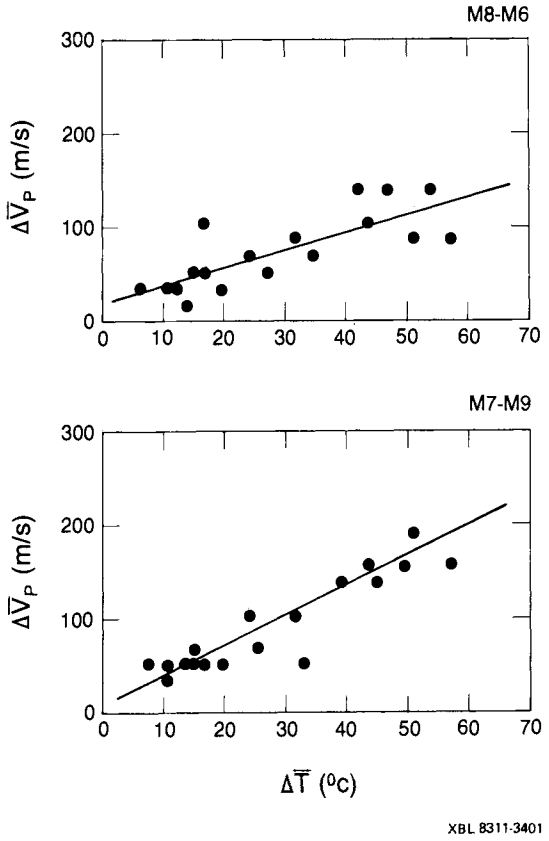

FIG. 22. Change of P-wave velocity as function of temperature change spatially from line 1 to line 39 on day 398 for cross-sections M8-M6 and M7-M9.

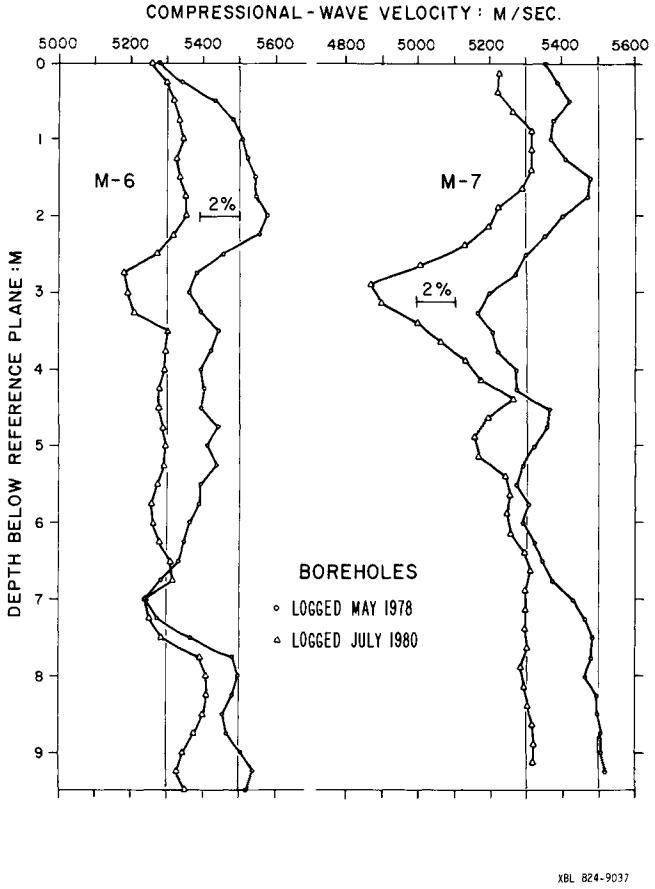

FIG. 23. Compressional wave velocities as function of depth in boreholes M6 and M7.

where k is the wavenumber in the x-direction, $\omega = 2\pi f$, where f is frequency, and the frequency-independent geometric spreading is given by the exponent n. Attenuation can be described by assuming the wavenumber to be complex:

$$k = k_r + i\alpha \tag{2}$$

to give

$$A(x, t) = A_0 x^{-n} e^{-\alpha x} e^{i(k_r x - \omega t)} \tag{3}$$

where in the x-direction the frequency-dependent attenuation coefficient $\alpha(f)$ is

$$\alpha(f) = \frac{\pi f}{QV}, \tag{4}$$

with the wave velocity $V = \omega/k_r$. For two different receiver positions x_1 and x_2 one obtains from the amplitude ratio

$$\ln\left[\frac{A(x_1)}{A(x_2)}\right] = f(\alpha_2(f)x_2 - \alpha_1(f)x_1) + n \ln\frac{x_2}{x_1}. \tag{5}$$

If

$$\ln\left[\frac{A(x_1)}{A(x_2)}\right]$$

is plotted as a function of f, the slope s of the line will give

$$s = \left[\frac{x_2}{Q_2 V_2} - \frac{x_1}{Q_1 V_1}\right]\pi = \left[\frac{t_2}{Q_2} - \frac{t_1}{Q_1}\right]\pi, \tag{6}$$

where t is traveltime. This was the formulation used for all Q data presented here with $1/Q_2$ being the attenuation for the reference spectrum. Clearly, equation (6) is an approximation, assuming no frequency-dependence for Q and ignoring dispersion. The purpose of its application is to quantify the spectral changes observed during the experiment.

The two cross-sections used for establishing the reference Q_α were M7-M8 and M8-M6. The angle between the two cross-sections was 29 degrees and the two cross-hole distances were 2.68 and 4.18 m, respectively. For observations at two distances along the same path, equation (6) reduces to

$$Q = \frac{\pi \delta x}{sV}, \tag{7}$$

where $\delta x = x_2 - x_1$, and the Q estimate is independent of the values of Q or V on the common path. Applying this method to cross-sections M7-M8 and M8-M6 yields a Q value of 57. However, the reference spectrum used for all the spectral ratio calculations was obtained from cross-section M7-M9 just before the heater was turned off. The reason for this selection is that this spectrum contains more high-frequency energy than any other spectrum and this assures that the slope always is

positive. A Q_α of 50 was chosen as a reasonable estimate for this standard spectrum. The sensitivity of equation (6) to the reference Q_2 is

$$\frac{dQ_1}{dQ_2} = \frac{t_2}{t_1}\left(\frac{Q_1}{Q_2}\right)^2, \tag{8}$$

or, in terms of attenuation,

$$\frac{dQ_1^{-1}}{dQ_2^{-1}} = \frac{t_2}{t_1}, \tag{9}$$

so that for either a high value of the reference Q or a large observation path relative to the reference path, the estimated Q_1 values are not strongly dependent upon the reference Q_2. In our case the former condition is assumed by selection of the high-Q reference spectrum. The Q_α values measured in the laboratory for saturated Stripa quartz monzonite under moderate pressure also indicated that $Q_\alpha = 50$ was a reasonable estimate (Paulsson, 1983).

The method was applied to all the P-wave data, and the Q_α values were obtained over the course of the experiment. Figure 25 shows the resulting data from the five monitor lines and the reference line. Each cross bar represents one data point: at the same time, the bar indicates that the standard deviation for the Q value estimate at that point is based on a least-squares linear fit of the natural logarithm of the spectral ratio as a function of frequency (Paulsson, 1983).

The first data points were taken two days before dewatering of the rock mass started, 41 days prior to heater turn-on. In comparison with the velocity data obtained on the monitoring lines, the Q_α values behaved quite differently. There was a gradual increase in the Q_α values during the entire course of the 398 day heater experiment, with little or no correlation with heater operation. However, there were several dips in this long-term increase. Over the inital period of 100 days heating there was little or no increase in Q_α. Over the following 30 days the Q_α values increased between 25 and 50 percent. Over the next 75 days the Q_α values decreased to a level just slightly above the initial level, except for the line M8-M9, which was farthest from heater H9. Over the next 60 days the Q_α values again increased. This behavior was repeated three times during the course of the heater experiment.

After the heater was turned off on day 398, the Q_α values measured over the four lines showed different modes of behavior. In line M7-M9 the Q_α values dropped over a period of 14 days from a value of 22 to a value of 12. In the two lines M7-M6 and M8-M6 there was very little change for the 150 days which followed heater turn-off. The Q_α values in line M8-M9 first decreased after turn-off, until day 425 when the Q_α values increased to reach the same value at day 490 as before heater turn-off. After day 490 all the Q_α values decreased gradually toward values similar to or below those recorded prior to the heater test.

Water inflow increased in some of the boreholes when the heater was turned on, and the increase lasted from 70 to 100 days. The decrease of the inflow after 100 days coincided with an increase in the Q_α values which had been constant through the first 100 days of heating. Dewatering ceased on day 545, resulting in a change in the H9 heater midplane Q_α values. For the three lines M8-M6, M8-M9, and M7-M6 the onset of the decrease in the Q_α values is apparent. For line M7-M9 there was a slower decrease in Q_α following the termination of the dewatering. This is probably due to the large initial decrease in Q_α value following heater turn-off. The value obtained 150 days after the termination of the dewatering, which represents the last data point, was considerably smaller than the value at termination. The calculated Q_α values from the 14 surveys in the two cross-sections reveal the complexity of the interaction of the temperature increase, fracture volume, pore pressure,

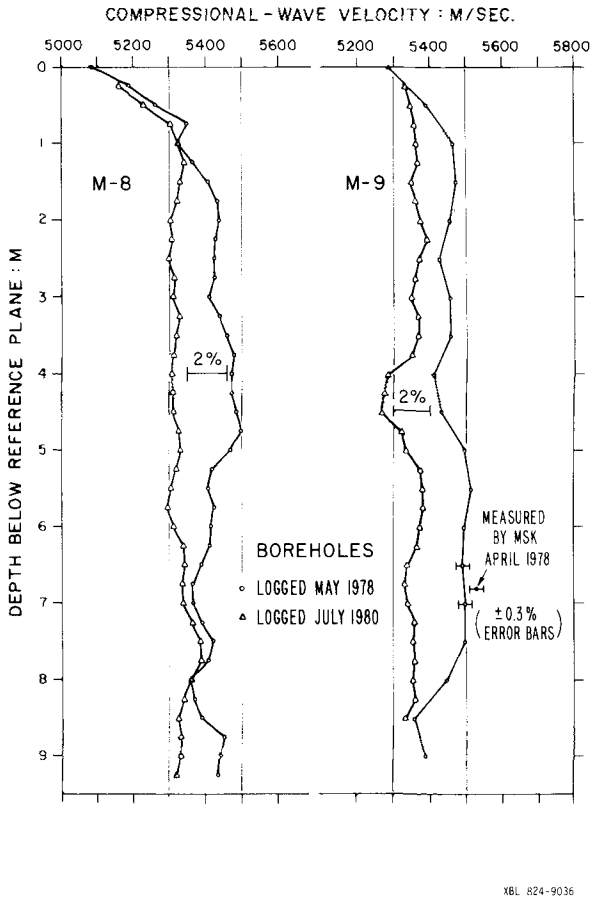

FIG. 24. Compressional wave velocities as function of depth in boreholes M8 and M9.

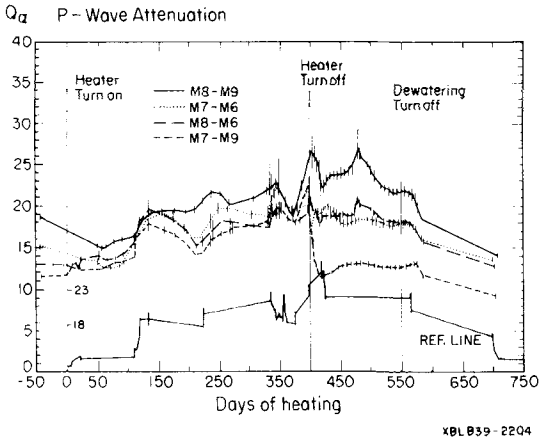

FIG. 25. Q_α for cross-hole signals over four monitor lines in the heater midplane and for the reference line. (Note that the scale for the reference line has a separate scale.)

geology, and direction of the propagation of the elastic waves.

The Q_α values from seven surveys from the M8-M6 cross-section are shown in Figure 18. For the three first surveys on days -7, 20, and 111 Q_α changed very little. For the fourth survey, on day 118, there was a small but noticeable change, mainly between depth lines 30 and 39. The increase in Q_α values in the lower part of the cross-section continued for survey 5 on day 341 and for survey 6 on day 420. The maximum Q_α values for survey 6 are found between depth lines 28 and 35, from 7 to 9 m below the drift floor. It appears as if the Q_α values below the bottom of the M holes tended to remain fixed. For surveys 5 and 6 in Figure 18 there are also increased Q_α values between 1 and 2 m below the drift floor, but values remain low in the upper meter, probably due to blasting damage in mining the drift. This effect is also seen in the velocity data from the same survey (see Figure 18). The lowest Q_α values during heating were found unexpectedly at the depths of the heater. However, in survey 6, on day 420 (22 days after heater turn-off), Q_α values had increased at and below the heater midplane. Survey 7, performed on day 704, revealed that Q_α values had returned to the original preheating values above and below the heater. At the heater level the Q_α values are slightly higher in survey 7 on day 704 than they were in survey 1 on day -7.

The Q_α values for the M7-M9 cross-section, shown in Figure 19, exhibit behavior generally similar to that seen in M8-M6, with some unique features. The Q_α values showed no change for the first three surveys on days 0, 13, and on day 20. For survey 4 on day 111 there were increases in Q_α around depth lines 20 and 32. In the fifth survey on day 349 the increase in Q_α was generally below the first meter. Survey 6 on day 419 (21 days

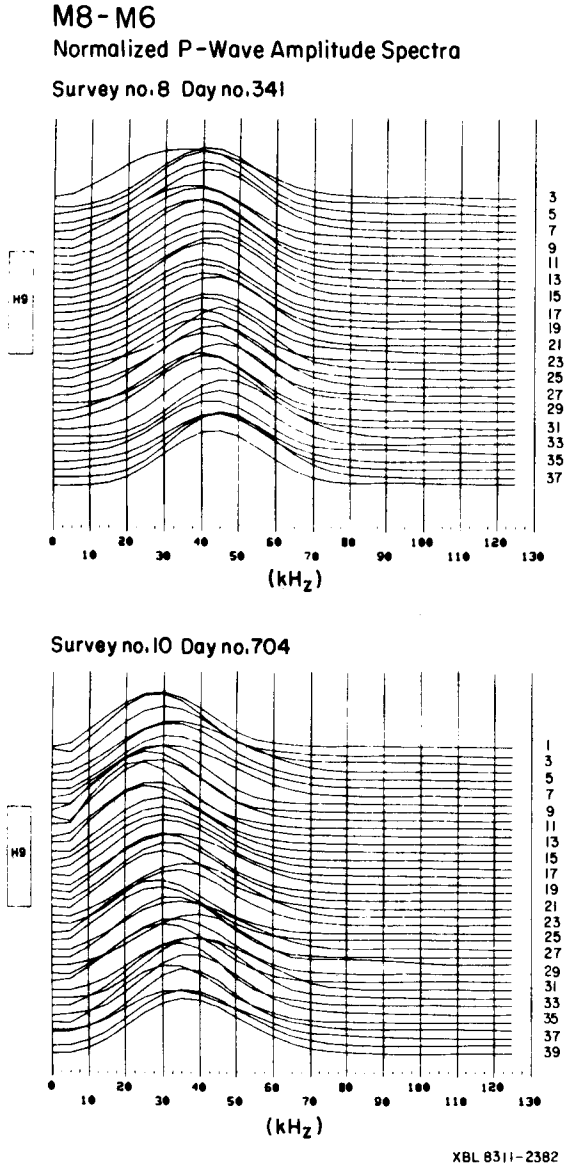

FIG. 26. Amplitude spectra for cross-section M8-M6 survey 8 (349 days after heater turn-on) survey, 10 (704 days after turn on of heater H9). The distance between each line represents a vertical spacing of 0.25 m.

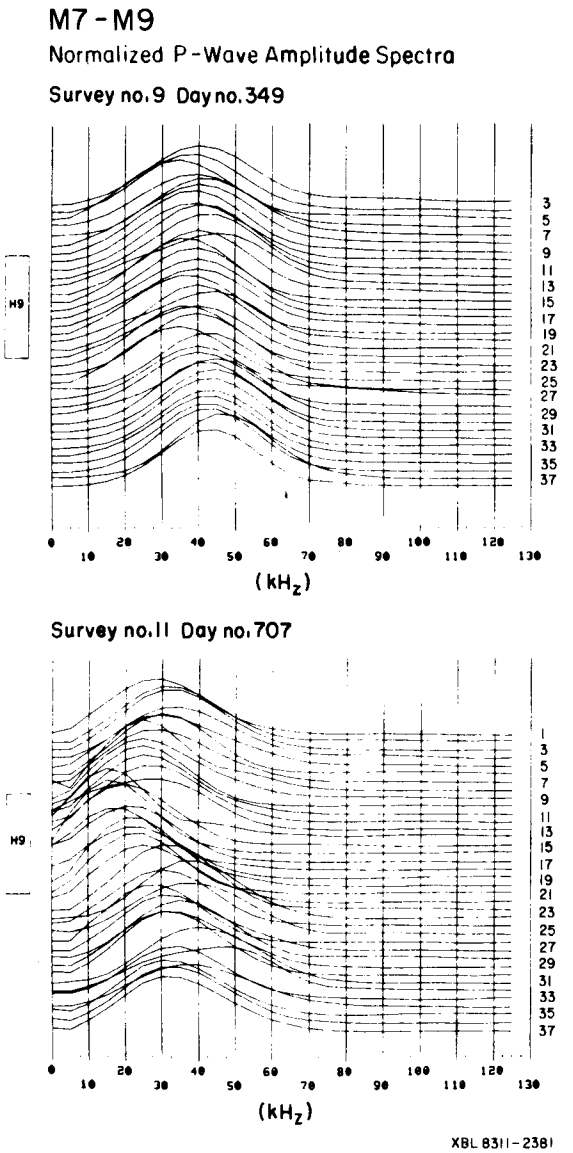

FIG. 27. Amplitude spectra for cross-section M7-M9 survey 9 (349 days after heater turn-on) and survey 11 (707 days after heater H9 was turned on). The distance between each line represents a vertical spacing of 0.25 m.

after the heater was turned off) is very interesting. The increase in Q_α continued at the upper and lower ends of the cross-section but, in the heater midplane, the Q_α values dropped. This is the only cross-section where this was observed. In survey 7 the Q_α values had returned to the original preheating values, except at the heater depth where Q_α values lower than preheating levels were observed. The same general pattern as seen for cross-section M8-M6 is also seen for cross-section M7-M9 in Figure 19.

In Figure 26 examples of amplitude spectra are shown for cross-section M8-M6 at two different times—day 341 when the heater still was in operation and day 704. The difference in the spectral content from which Q changes were calculated is apparent. Figure 27 shows similar spectra for cross-section M7-M9, during heater operation and at day 707, the last data collected in this cross-section.

The highest temperatures in the experiment were found between 2 and 6.25 m below the floor of the full-scale drift. The effects on Q are complex, representing the interaction of several processes being driven by the heating and related thermal expansion in the vicinity of the H9 hole.

The significant apparent effect of dewatering on attenuation of the P-waves was largely unexpected. Q_α values for the first surveys in the six cross-sections show no or little correlation with the P-wave velocities or with the geologic features mapped between the boreholes. The four lines which pass close to the heater—M7-M6, M7-M8, M8-M6, and M7-M9—all show Q_α values increasing with time in the lower parts of the cross-sections. When dewatering ceased, Q_α values returned very nearly to the values measured during the first surveys.

DISCUSSION AND CONCLUSIONS

Salient features of the Stripa study are summarized as follows.

(1) Changes in traveltimes and attenuation of high-frequency P-waves were measured underground in the rock around an electrical heater over a period of 704 days, comprising 398 days of heating followed by 306 days of cooling, during which time the rock underwent changes in temperature and thermally induced stresses, returning eventually to its initial conditions.

(2) For a period spanning the thermal cycle the rock was drained of expelled water by emptying the boreholes around the heater.

(3) Changes in the measured P-wave traveltimes correlate well with changes in mean rock temperatures, higher temperatures producing shorter traveltimes.

(4) Changes in P-wave traveltimes varied with the orientation of the seismic path, the smaller changes occurring in the direction of greater measured compressive stress.

(5) Zones of calcite-filled joints showed up as low-velocity zones before heating and as regions of permanently reduced velocity as a result of heating.

(6) Attenuation, measured as Q_α changed from values of 10 to 15 to as much as 35 during the heating cycle, but there is no correlation between changes in Q and changes in rock temperatures, although changes in Q appear to be related to thermal expansion-driven dewatering of the rock during the heater experiment.

A model

To analyze this series of experiments, we attempt to relate observed effects to changes in physical properties. Thermal expansion of the rock around the heater hole increases the compressive stress far beyond the zone actually heated, with resultant closure of cracks at large distances. The pore fluid with a higher coefficient of thermal expansion than that of the rock, adds its own effects to the overall system response to heating. The Stripa granite, typical of rocks which are being considered as host rock for nuclear waste repositories, has a low permeability, estimated at about 10^{-13} cm^2 (Gale et al., 1982). Such a low permeability, decreased further by thermal expansion, apparently inhibits dissipation of the increasing pore-fluid pressure by flow when the rock mass is subjected to rapid heating.

The effect of heating is the formation of a zone with reduced permeability around the heater. Where the water can be expelled from the rock, such as around the boreholes, the fractures can close due to thermal expansion. The water expulsion data support this hypothesis, showing a large increase in water inflow to the holes just after the heater was turned on. This model for fracture closure can explain the observed changes in velocity and attenuation near the heater and at greater distances from the heater where dissipation of the pore water pressure takes longer, due to longer fluid paths to the drain sites.

Both velocity and attenuation show major changes throughout the experiment. However, there are differences between the velocities and the attenuation in the response times to various stimuli. There are two dominant processes operating during the experiment: (1) the heating of the rock mass, and (2) its dewatering by the 22 boreholes. While 95 percent of the final temperature increase 0.20 m from the heater was reached 62 days after the heater was turned on, the water expulsion process continued throughout the entire experiment, and the rate of water removal after the initial heavy flow was in most boreholes fairly constant throughout the experiment. The two measured quantities, the P-wave velocity V_p and the attenuation of P-waves Q_α, are both sensitive to changes in stress and to the degree of fluid saturation. The compressional wave velocities are very sensitive to changes in stress in the region 0 to 20 MPa. In this range the fractures are in the process of closing. The attenuation Q_α is more sensitive to the final process of fracture closure as the surfaces come into close physical contact.

Velocity and attenuation changes in the heater midplane

The seismic waves measured traveled several meters though regions having different states of temperature, stress, and fluid saturation. The velocity and the attenuation changes are average values over the distances traveled. Changes with time in the mean temperatures over the four lines in which changes of V_p and Q_α have been measured are shown in Figure 8. For three of the four lines, 95 percent of the total mean temperature increase was reached after 80 days of heating. The time constants for the cooling curves are approximately the same as for heating for all four lines. The water table is approximately 10 m below the surface around the Stripa mine, so rock in the test area was fully saturated at the beginning of the experiment.

V_p for the monitor lines (Figure 16) shows a regular behavior

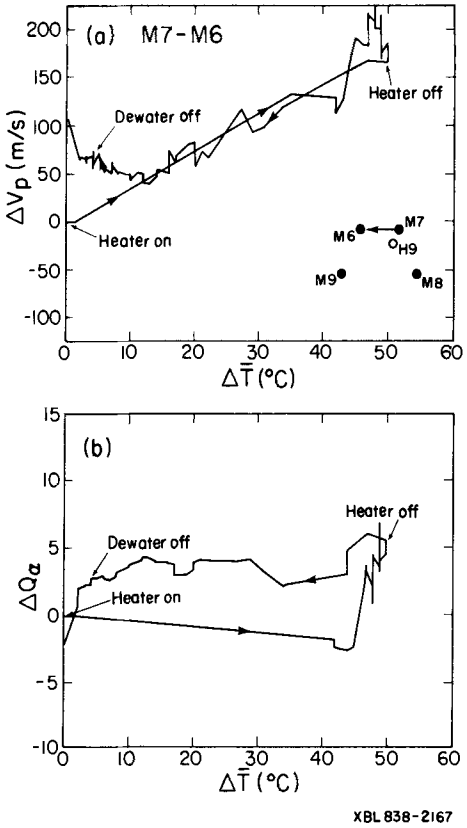

FIG. 28. Change in compressional wave velocity V_p and in Q_α as functions of change in mean temperature in line M7-M6. Times of termination of the heating and the dewatering are marked.

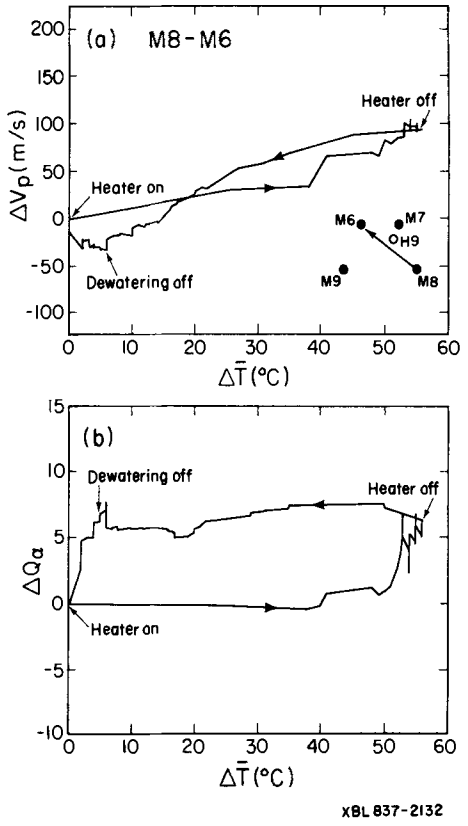

FIG. 30. V_p and Q_α changes in M8-M6, as in Figure 28.

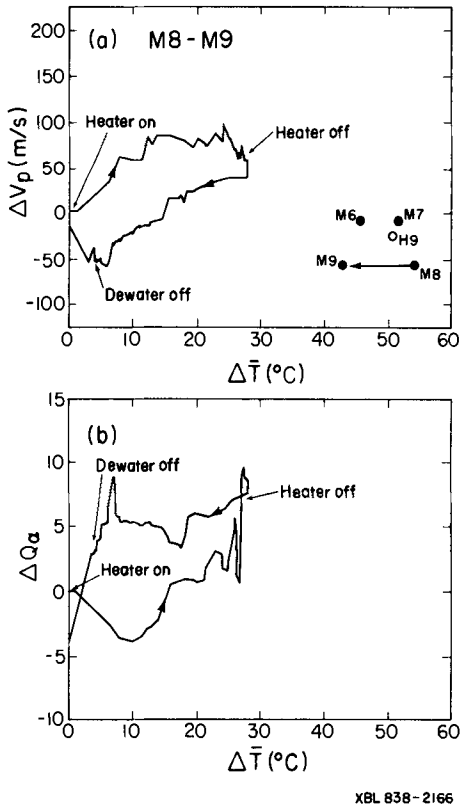

FIG. 29. V_p and Q_α changes in M8-M9, as in Figure 28.

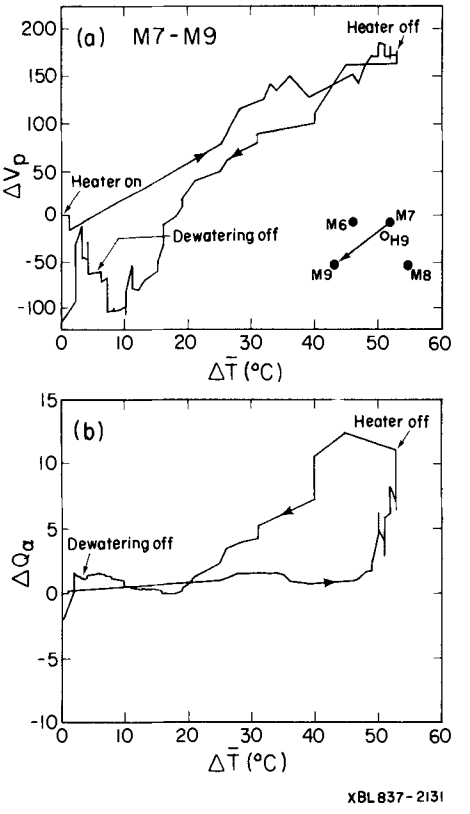

FIG. 31. V_p and Q_α changes in M7-M9, as in Figure 28.

with temperature, increasing 5 to 10 percent from the ambient levels, depending upon the direction of transmission and decreasing upon turn-off of the heater. For at least one line, M7-M9, the postheating values are clearly lower than the values observed prior to the experiment, suggesting permanent damage to the fractures under the high thermal compressive stress.

The variations of Q_α calculated over the four monitor lines are less regular than for the velocities. The variations can be explained by an increase of pore pressure to the point where tensile strength of the rock or an adjacent fracture is reached, allowing a subsequent decrease in pore fluid pressure as fluid flows into the newly created pore space. This mechanism will produce a decrease in effective stress, followed by an increase.

In Figures 28, 29, 30, and 31 V_p and Q_α are shown as functions of mean temperature in the midplanes of the four monitor lines. A common feature in the four figures is that Q_α values remain unchanged as the mean temperatures increase. After the temperature change reaches about 40° C the Q_α values slowly increase 5 to 10 units as the temperatures reach maximum values. This behavior at the higher temperatures is interpreted to be due to the low permeability in the heated zone and the resulting slow expulsion of water into boreholes as the rock mass is compressed. When the heater is turned off, the Q_α values stay at the higher levels until the dewatering is complete, except that for the M7-M9 line there appears to have been a rapid enough thermal contraction of the rock for the fractures to have become partially saturated. Line M7-M9 passes closest to the heater and thus through rock with the highest temperature (128°C).

The V_p values increase with temperature in all four lines. For line M7-M6 the increase is not linear with temperature. This may be due to thermally induced pore pressure which decreases the effective stress and prevents velocities from rising. The dip in the increase of V_p (seen in Figure 16) for this line represents retardation of velocity increase with temperature. The same effect, less pronounced, can also be seen for the other lines in Figure 16.

For the two main lines, M8-M6 and M7-M9, the linear relationship between temperature and velocity is very near that presented in Table 2 for spatially distributed data on day 398, where the rates of increase for the two lines are 2 m/s/°C and 4 m/s/°C, respectively. It is satisfying that the two data sets give nearly identical results for the velocity-temperature relationship for the two different lines, even though one method looks at all temperatures in the section at a given time, while the other method follows the velocity change on a given line as the temperature varies with time. The difference between the lines is attributed to the different field stresses in the two directions.

Summary

Measurements of the velocity and attenuation properties of high-frequency ultrasonic seismic waves transmitted between boreholes in the heated zone of a rock mass constitute an effective seismic technique for detailed rock mechanical investigations of an underground mined facility. Specific results of the field work applying such a method in the Stripa mine are as follows.

(1) Thermally induced velocity changes can be located by cross-hole seismic measurements between two boreholes in the rock mass.

(2) *P*-wave velocities provide a quantitative measure of changes in the fracture porosity of the medium, using measured velocities and the modal composition of the rock.

(3) *P*-wave velocity variations upon dewatering have a directional component, i.e., the porosity changes indicated vary systematically with direction of the cross-section. The total porosity of the Stripa quartz monzonite was estimated to be 1.5 percent. The effective porosity varied between 0.16 and 0.23 percent, with the higher value obtained in the M8-M6 section, a direction which is roughly perpendicular to most of the fractures in the rock mass.

(4) The *P*-wave velocity increases linearly with temperatures up to 130°C. The rate of change of velocity with temperature varies from 2.0 to 4.0 m/s/°C for mean temperatures up to 66°C. The largest velocity changes were found in the general direction of the minimum horizontal principal stress, as inferred from geologic evidence such as faulting and pegmatite dikes, and from in-situ stress measurements.

(5) *P*- and *S*-wave velocities can be used to assess thermal damage of a rock mass and the extent of the disturbed zone due to heating. Damage to the rock mass, as indicated by permanently reduced *P*-wave velocities, was observed as far as 2.1 m from the 3.6 kW H9 heater. The temperature increase at this distance was less than 35°C.

(6) Attenuation properties change rapidly at some point during the process of fracture closure in the heating cycle. Laboratory tests indicate that a similar rapid decrease in attenuation occurs when the fracture asperities first come into contact. This suggests that attenuation measurements offer a means of monitoring fracture closure.

The most important result of this work is the demonstration that a small-scale field experiment was successful in monitoring important parameters of the rock which could not be obtained by laboratory experiments. This experimental work can serve as a prototype data base for guiding implementation of high-frequency seismic monitoring systems in full-scale repositories or in other underground facilities where the medium integrity must be known and maintained.

ACKNOWLEDGMENTS

B. N. P. Paulsson acknowledges M. S. King for his instrumental support for this research. Lawrence Berkeley Laboratory provided major support for this work through Department of Energy contract no. DE-AC03-76SF00098. Karnbranslesakerhet, Inc. Sweden, provided support for the field work. The Mineral Institute at the University of California, Berkeley provided support for B. N. P. Paulsson during the final completion stages of the presented work.

REFERENCES

Aki, K., Fehler, M., Aamodt, R., Albright, J., Potter, R., Pearson, C., and Tester, J., 1982, Interpretation of seismic data from the hot dry rock fracture experiment at Los Alamos Scientific Laboratories: J. Geophys. Res., **87**, 936–944.

Andersson, B., and Halen, P. H., 1979, Mining methods used in the underground tunnels and test room at Stripa: Lawrence Berkeley Lab. Rep., LBL-7081, SAC-8.

Carlsson, H., 1978, Stress measurements in the Stripa granite: Lawrence Berkeley Lab. Rep., LBL-7078, SAC-4.

Chan, T., Binnal, E., Nelson, P. N., Stolzman, R., Wan, O., Weaver, C., Ang, K., Braley, J., and McEvoy, M., 1980, Thermal and thermomechanical data from in-situ heater experiments at Stripa, Sweden: Lawrence Berkeley Lab. Rep., LBL-11477, SAC-29.

Chan, T., Cook, N. G. W., and Tsang, C. F., 1978, Theoretical temperature fields for heater project at Stripa: Lawrence Berkeley Lab. Publ. 7082, Berkeley, CA.

Doe, T., 1982, Determination of the state of stress at the Stripa mine, Sweden: Earth Sci. Div. Annual Rep., Lawrence Berkeley Lab.

Doe, T. W., Ingevald, K., Strindell, L., Haimson, B. C., and Carlsson, H., 1981, Hydraulic fracturing and overcoring stress measurements in a deep borehole at the Stripa test mine, Sweden: Proc., 22nd U. S. Rock Mechanics Symp., Mass. Inst. Technology, 373–378.

Fehler, M., 1981, Changes in *P*-wave velocity during operation of a hot dry rock geothermal system: J. Geophys. Res., **86**, 2925–2928.

——— 1982 Using dual-well seismic measurements to infer the mechanical properties of a hot dry rock geothermal system: J. Geophys. Res., **87**, 5485–5494.

Gale, J. E., Witherspoon, P. A., Wilson, C. R., and Rouleau, A., 1982, Hydrogeological characterization of the Stripa site: Presented at the workshop on in-situ experiments in granite associated with geological disposal of radioactive waste, Stockholm, Sweden, October 25–27.

Jaeger, J. C., and Cook, N. G. W., 1979, Fundamentals of rock mechanics, 3rd ed.: Chapman and Hall, Wiley and Sons.

King, M. S., and Paulsson, B. N. P., 1982, Acoustic borehole logging in a granitic rock mass subjected to heating: Issues in rock mechanics, 39–46, 23rd Symp. on Rock mechanics, Berkeley, CA, August 25–27.

McDonal, F. J., Angona, F. A., Mills, R. L., Sengbush, R. L., Van Nostrand, R. G., and White, J. E., 1958, Attenuation of shear and compressional waves in Pierre shale: Geophysics, **23**, 421–439.

Nelson, P. H., Rachiele, R., Remer, J. S., and Carlsson, H., 1981, Water inflow into boreholes during the Stripa heater experiments: Lawrence Berkeley Lab. Rep., LBL-12574, SAC-35.

Paulsson, B. N. P., Nelson, P., and Kurfurst, P. J., 1981, Characterization of the discontinuities in the Stripa granite—the full scale experiment drift: Lawrence Berkeley Lab. Rep., LBL-9063.

Paulsson, B. N. P., 1983, Seismic velocities and attenuation in a heated underground granitic repository: Ph. D. thesis, Univ. of California, Berkeley.

Toksöz, M. N., Johnston, D. H., and Timur, A., 1979, Attenuation of seismic waves in dry and saturated rocks; 1. Laboratory measurements: Geophysics, **44**, 681–690.

Tullos, F. N., and Reid, A. C., 1969, Seismic attenuation of Gulf Coast sediments: Geophysics, **34**, 516–528.

Witherspoon, P. A., Cook, N. G. W., and Gale, J. E., 1980, Progress with field investigations at Stripa: Lawrence Berkeley Lab. Rep., LBL-10559, SAC-27.

Witherspoon, P. A., and Degerman, O., 1978, Swedish-American cooperative program on radioactive waste storage in mined caverns: Lawrence Berkeley Lab. Rep., LBL-7049, SAC-01.

Wollenberg, H., Flexer, S., and Andersson, L., 1981, Petrology and radiogeology of the Stripa pluton: Lawrence Berkeley Lab. Rep., LBL-11654, SAC-36.